

ORIGINAL ARTICLE**On the parameter refinement of inflated exoplanets with large radius uncertainty based on TESS observations**X. Alexoudi*^{1,2,3}¹Leibniz-Institut für Astrophysik Potsdam (AIP), Potsdam, Germany²Universität Potsdam, Institut für Physik und Astronomie, Potsdam, Germany³Potsdam Graduate School, Potsdam, Germany**Correspondence**

*Email: xalexoudi@aip.de

arXiv:2201.02133v1 [astro-ph.EP] 6 Jan 2022

We revisited ten known exoplanetary systems using publicly available data provided by the Transiting Exoplanet Survey Satellite (TESS). The sample presented in this work consists of short period transiting exoplanets, with inflated radii and large reported uncertainty on their planetary radii. The precise determination of these values is crucial in order to develop accurate evolutionary models and understand the inflation mechanisms of these systems. Aiming to evaluate the planetary radius measurement, we made use of the planet-to-star radii ratio, a quantity that can be measured during a transit event. We fit the obtained transit light curves of each target with a detrending model and a transit model. Furthermore, we used emcee, which is based on a Markov chain Monte Carlo approach, to assess the best fit posterior distributions of each system parameter of interest. We refined the planetary radius of WASP-140 b by approximately 12%, and we derived a better precision on its reported asymmetric radius uncertainty by approximately 86% and 67%. We also refined the orbital parameters of WASP-120 b by 2σ . Moreover, using the high-cadence TESS datasets, we were able to solve a discrepancy in the literature, regarding the planetary radius of the exoplanet WASP-93 b. For all the other exoplanets in our sample, even though there is a tentative trend that planetary radii of (near-) grazing systems have been slightly overestimated in the literature, the planetary radius estimation and the orbital parameters were confirmed with independent observations from space, showing that TESS and ground-based observations are overall in good agreement.

KEYWORDS:

techniques: photometric, stars: WASP-140, WASP-136, WASP-113, WASP-120, WASP-93, HAT-P-16, WASP-123, WASP-76, WASP-20, WASP-108, planetary systems

1 | INTRODUCTION

The field of exoplanets is a rapidly advancing domain in modern astrophysics. Surveys and missions were dedicated through the years with joint ground- and space-based efforts in the discovery of exoplanets and the characterization of their interiors (e.g. The Hungarian Automated Telescope Network (HATNet) project (Bakos 2018), the SuperWASP: Wide

Angle Search for Planets project (Street et al. 2003), the CoRoT project (Barge, Baglin, Auvergne, & CoRoT Team 2008) and the Hubble Space Telescope (HST)). The results of these endeavors has shown that exoplanets are not similar to the planets of our solar system; increasing this way the interest of the scientific community to investigate further these unknown exotic worlds. For example, the Kepler mission (Borucki et al. 2010) (and later on the K2 mission

(Howell et al. 2014), a follow-on to the Kepler mission), provided thousands of transiting systems, where the planet orbits its host star on an edge-on orbit, as seen by an observer on the Earth. Those systems included Earth-like planets, Neptune-sized, and interestingly large gaseous planets of the size of Jupiter at short orbital periods. However, most of Kepler’s targets are faint stars, and the atmospheric characterization of large gaseous transiting exoplanets is favorable only for the brightest candidates.

One mission that is focused specifically on bright targets (5% on brighter than $V_{mag} = 8$) is the Transiting Exoplanet Survey Satellite (TESS), which was launched in 2018 (Ricker et al. 2015) and it is scheduled to fixate its detectors on more than 100 exoplanets. For more than three years, TESS has been observing the night sky and has been providing datasets of photometric monitoring of bright stars and their planets, triggering follow-up studies by ground-based facilities and setting up the challenge for future space-born missions (e.g. the James Webb Space Telescope, JWST, of Gardner et al. (2006)).

The radii of inflated hot Jupiters, strongly affected by the irradiation of their host stars, extend beyond the typical Jupiter radius size. They can be determined from uninterrupted high-quality photometric light curves, always with respect to their host star radius measurement. The dimming in the brightness of these stars is larger for transiting gas giants with extended inflated radii. Even though, the planet radius estimation is derived straightforward from the planet-to-star radii ratio measurement during a transit event, the uncertainty on this measurement can be constrained significantly due to different factors; from unknown systematic errors to incomplete datasets, or a different approach on the methodology that was used for the transit light curve analysis. The required precision for the planetary radius measurement can contribute to the general understanding of the inflation scenarios taking part on different exoplanets.

Some of the most prominent mechanisms able to trigger the effect of inflation on gas giant exoplanets are: the irradiating flux sourcing from the host star itself, that heats up the planet and increases its equilibrium temperature (Guillot & Showman 2002), the ohmic heating mechanism (Laughlin, Crismani, & Adams 2011), as a result from the coupling of the atmospheric flows with the magnetic field of the planet, the kinetic heating (a more direct mechanism), as some incident flux turns into kinetic energy and eventually into thermal energy that heats up the atmosphere. Last but not least, another mechanism is the tidal heating promoted by the circularization of the planetary orbit (Bodenheimer, Lin, & Mardling 2001; Lecote, Chabrier, Baraffe, & Levrard 2010). Evolutionary models that predict the formation mechanisms of inflated exoplanets can gain in robustness with the precise measurements

of the key physical and orbital parameters of those exotic systems, and conclude to a suitable explanation for the applied inflation mechanism.

Moreover, studies on transiting exoplanets can yield an accurate planetary radius, that in combination with high precision radial velocity (RV) observations, can provide a mass for the planet, hence a mean density estimation which gives important information regarding the internal structure of these planets. Furthermore, the precise radius estimation and the distance from their hosts, can give insights on the gravitational potential of the planets and their equilibrium temperature. Consequently, those computations are useful in transmission spectroscopy because they provide an estimation of the extension of an exoplanetary atmosphere, if it is present. The correct characterization of this, is based on the investigation of the planetary to stellar radii ratio over different wavelengths of observation, known as the transmission spectrum. The employment of incorrect parameters in the light curve analysis can compromise the structure of the spectrum and yield misplaced slopes (Alexoudi et al. 2020). TESS is expected to contribute to those studies by providing precise physical and orbital parameters derived from high-quality high-cadence datasets.

Motivated by the aforementioned capabilities of TESS, we obtained a sample of inflated hot giants, orbiting bright stars in short close-in orbits, and proceeded with a parameter refinement of those systems since their parameters have not been up-to-date for more than three years (see Table 1). The dates of the last update are presented as registered at the NASA Exoplanet Archive¹. In this work, we focused on exoplanets with the largest reported planetary radius uncertainty, and we expected TESS to ameliorate our knowledge on the planetary radii of those systems and their physical properties. The aim is to provide the most accurate parameterization of these systems and quantify TESS’s capabilities in comparison to the ground-based facilities.

The structure of this paper is the following: Section 2 presents the TESS observations of each exoplanet of our sample. In Section 3, we describe the reduction method that was employed for the analysis of these datasets and in Section 4, we demonstrate the adopted methods in order to derive the system parameters of our targets. In Section 5, we present our results and in Section 6 we discuss the impact of these findings regarding the characterization of hot giant exoplanets. In the end, in Section 7, we provide a summary and the conclusions of this entire work.

¹exoplanetarchive.ipac.caltech.edu

Exoplanet	TESS mag	P (d)	$R_p(R_J)$	Date of last update	Publication
WASP-140 b	10.3	2.2	$1.440^{+0.42}_{-0.18}$	2016-11-30	Hellier et al. (2017)
WASP-136 b	9.5	5.2	1.380 ± 0.160	2016-11-30	Lam et al. (2017)
WASP-113 b	11.2	4.5	$1.409^{+0.096}_{-0.140}$	2016-07-14	Barros et al. (2016)
WASP-120 b	10.6	3.6	1.473 ± 0.096	2016-06-01	O. D. Turner et al. (2016)
WASP-93 b	10.6	2.7	1.597 ± 0.077	2016-09-06	Hay et al. (2016)
HAT-P-16 b	10.8	2.8	1.289 ± 0.066	2014-05-14	Buchhave et al. (2010)
WASP-123 b	10.4	3.0	1.318 ± 0.065	2016-06-01	O. D. Turner et al. (2016)
WASP-76 b	9.0	1.8	$1.830^{+0.060}_{-0.040}$	2016-01-20	West et al. (2016)
WASP-20 b	10.7	4.9	1.459 ± 0.057	2015-03-05	Anderson et al. (2015)
WASP-108 b	11.2	2.7	1.215 ± 0.04	2014-10-29	Anderson et al. (2014)

TABLE 1 The sample of this work. The sample selection is based on exoplanets with inflated radii ($R_p > 1.2R_J$), that orbit relatively bright stars (TESS mag < 12), in short orbital periods ($P < 5$ days). The planetary radius of each target has last been updated between the years 2014 and 2017, and therefore its refinement is necessary. The targets are sorted by the uncertainty on R_p with a decreasing order.

2 | OBSERVATIONS

Our sample consists solely of TESS observations, spanning the period of 2018-2020. We re-visited ten inflated hot giants (nine hot Jupiters and one Saturn-sized planet) using the publicly available, two-minute cadence data of TESS. The complete list of the observations is presented in Table 2. The obtained light curves were processed by the Science Processing Operations Center (SPOC) pipeline, based on the work of Jenkins et al. (2016). We made use of the PDCSAP_FLUX, which is the Pre-search Data Conditioning SAP flux, in order to access SPOC’s data. PDCSAP_FLUX has an advantage over the simple aperture photometry (SAP_FLUX), because of the use of the Cotrending Basis Vectors (CBVs). CBVs remove longstanding systematic trends and provide better data quality (Tenenbaum & Jenkins 2018). Another approach would be to use the light curves derived from the data validation timeseries (DVT) files as in Ridden-Harper, Turner, & Jayawardhana (2020), however a standard process for the analysis of TESS data is the use of the PDC light curve (Espinoza et al. 2020; Shporer et al. 2019; J. D. Turner, Ridden-Harper, & Jayawardhana 2021). With the use of PDCSAP products, we obtained light curves corrected for pointing and focus related systematics, for the cosmic rays’ contribution to the detector, for persistent outliers and flux contamination (Jenkins et al. 2016). Moreover, we performed a further selection criterion on the datasets by masking out the bad cadences. During the observations some pixels may be contaminated by various effects e.g. spacecraft is in coarse point, reaction wheel desaturation event, cosmic ray detected, stray light from the Earth or Moon (see a complete set of such effects in Table 32 in Tenenbaum & Jenkins (2018)). To account for this, we used

a conservative setting (in the lightkurve package - Lightkurve Collaboration et al. (2018)) in our analysis that excludes cadences with data-quality issues (Littlefield et al. 2019). All the cadences considered in this work are of high-quality, are products of the SPOC pipeline, and publicly available at the Mikulski Archive for Space Telescopes (MAST) ².

3 | DATA ANALYSIS

We made use of Lightkurve (Lightkurve Collaboration et al. 2018), a Python package for Kepler and TESS data analysis. We cleaned additionally the light curves from outliers to the 6σ level, and normalize them by the median. We applied a further correction in the light curves by removing additional trends using the flatten method of the lightkurve package. This correction removes long-term trends using a Savitzky-Golay filter. We applied a window length of the filter of 1501 points and a break tolerance (in order to account for any large gaps in time) of 50. For each individual light curve of each sector, we applied a second order time-dependent polynomial, aiming to remove any remaining trends. We made use of the Bayesian Information Criterion, BIC (Schwarz 1978), to determine the best detrending model for our transit light curve fitting (Mallonn et al. 2016, 2015), and we concluded to a second order time-dependent polynomial that yields a smaller BIC value. In the end, we folded the light curves to a common transit mid-time reference of zero. Then, we used a combination of a detrending polynomial for the folded light curve and the Bad-Ass Transit Model cAlculationN (BATMAN software by

²<https://archive.stsci.edu/>

Target	Sector	Start Date	End Date	Cycle	Camera
WASP-140 b	4	2018 – Oct – 18	2018 – Nov – 15	1	2
	5	2018 – Nov – 15	2018 – Dec – 11	1	2
	31	2020 – Oct – 21	2020 – Nov – 19	3	2
WASP-136 b	29	2020 – Aug – 26	2020 – Sept – 22	3	1
	42	2021 – Aug – 20	2021 – Sep – 16	4	2
WASP-113 b	23	2020 – Mar – 18	2020 – Apr – 16	2	3
	24	2020 – Apr – 16	2020 – May – 13	2	2
WASP-120 b	4	2018 – Oct – 18	2018 – Nov – 15	1	3
	5	2018 – Nov – 15	2018 – Dec – 11	1	3
	30	2020 – Sep – 22	2020 – Oct – 21	3	3
	31	2020 – Oct – 21	2020 – Nov – 19	3	3
WASP-93 b	17	2019 – Oct – 07	2019 – Nov – 02	2	2
HAT-P-16 b	17	2019 – Oct – 07	2019 – Nov – 02	2	2
WASP-123 b	13	2019 – Jun – 19	2019 – Jul – 18	1	1
	27	2020 – Jul – 04	2020 – Jul – 30	3	1
WASP-76 b	30	2020 – Sep – 22	2020 – Oct – 21	3	1
	42	2021 – Aug – 20	2021 – Sep – 16	4	3
WASP-20 b	2	2018 – Aug – 22	2018 – Sep – 20	1	1
	29	2020 – Aug – 26	2020 – Sep – 22	3	1
WASP-108 b	11	2019 – Apr – 22	2019 – May – 21	1	2
	37	2021 – Apr – 02	2021 – Apr – 28	3	2
	38	2021 – Apr – 28	2021 – May – 26	3	2

TABLE 2 The TESS observations of each target, that were used in this work. We provide information on the sector, on the date, the observing cycle of each observation and the camera that was used. For many of the targets, there were available datasets of observations from multiple sectors.

Kreidberg (2015)) in order to fit our data. We adopted initial model parameters as defined for each exoplanet from their discovery papers and used the Barycentric Julian Date as the Barycentric Dynamical Time (BJD_{TDB}) standard for the mid-time, as it is generally recommended being used in practice for astrophysical events (Eastman, Siverd, & Gaudi 2010). We made use of the quadratic limb darkening law (Howarth 2011), and employed coefficients from the limb darkening calculator of the Exoplanet Characterization Toolkit³. We preferred limb darkening coefficients (LDCs) calculated with the ATLAS stellar atmospheric model grids, because there is an offset between the theoretical and the observed TESS LDCs when using the PHOENIX models, while using the ATLAS models there is a significantly smaller offset (Claret 2017). Then, we chose the traditional Cousins I - band, for the wavelength band for which to obtain the LDCs, because the TESS detector bandpass is centered on 786.5 nm⁴. And finally, we proceeded with the light curve fit process. That being the case,

we kept all the parameters fixed to their theoretical values, except the time of the mid-transit T_0 , the orbital inclination i , the semi major axis normalized in stellar radii a/R_s , the ratio of the planet to star radii R_p/R_s , and the three terms of the time polynomial c_0, c_1 and c_2 . The orbital period P , the eccentricity e and the limb darkening coefficients remained fixed to their theoretical values during the fitting process. The free parameters were fit through the maximum likelihood optimization. For this purpose, we used the "optimize" module from SciPy⁵, in order to apply a numerical optimization to the likelihood function and derive the parameters that maximize it. We made use of the maximum likelihood estimation of the free model parameters and employed the emcee⁶ approach (Foreman-Mackey, Hogg, Lang, & Goodman 2013) to fit the combined transit model on the data and obtain posterior distributions for each parameter with errors. We used uniform prior values from where the emcee can draw samples in order to define the posterior values. The final probability function is a sum of the prior

³exoctk.stsci.edu/limb_darkening

⁴heasarc.gsfc.nasa.gov/docs/tess/the-tess-space-telescope.html

⁵<https://docs.scipy.org/doc/scipy/reference/optimize.html>

⁶emcee.readthedocs.io/en/stable/

function and the likelihood function. We set the initialization of 30 walkers around the maximum likelihood estimations of each parameter and then run 20000 iterations. We access the samples using the “EnsembleSampler.get chain” method and identify the parameter values for each walker and for each iteration of the chain. The walkers initially wander around the maximum likelihood values of each parameter, and then very quickly start to converge towards the full posterior distribution. There is a burnt-in phase of around 10000 steps. We ensured convergence of the chains with the integrated autocorrelation time τ metric, which computes the autocorrelation time of the emcee. Usually, chains longer than $50 \times \tau$ are sufficient and the burnt-in phase of 10000 steps ensured convergence for all the chains of the analyses of all our targets. Then, we thinned each chain and flatten it, so we would obtain a final flat list of samples. We present the best-fit parameters for each target in corner plots, where we can see the projections of the posterior probability distributions of our parameters. The 2-D histograms show the marginalized distribution of each. We used the uncertainties based on the 16th, 50th and, 84th percentiles of the samples. These confidence intervals correspond to $\pm 1\sigma$ for a Gaussian posterior distribution. The best fit of the modeled transit light curves and the corner plots of the analysis of each exoplanet of our sample are presented in the Appendix A.

4 | DERIVATION OF THE PHYSICAL PARAMETERS

The investigation of inflated giant exoplanets with high-quality photometric TESS observations allows for a more concrete estimate of the properties of those systems. In our analysis, we adopted the values for the stellar radius R_s , the e and the RV semi-amplitude of the stars K_* , of these systems from their discovery papers. The newly derived parameters with TESS: T_0 , R_p/R_s , a/R_s , i , can provide a refined measurement on their planetary surface gravitational acceleration, g_p and on their equilibrium temperature, T_{eq} . The updated R_p , being a direct connection to the density of these exoplanets, can yield a first characterization of their internal structure. Moreover, regarding the atmospheric characterization of these systems, we calculated a quantity that describes the relative atmospheric scale height of their atmospheres, H . With the measurement of H in km, we can define the extension of the absorbing annulus due to the planet’s atmosphere. We made use of the equations from Southworth, Wheatley, & Sams (2007), Southworth et al. (2010), Winn et al. (2010), Seager (2011), O. D. Turner et al. (2016), Alexoudi et al. (2018), in order to compute all these quantities.

The surface gravitational acceleration is given by Eq. 1:

$$g_p = \frac{2\pi}{P} \left(\frac{a}{R_p} \right)^2 \frac{\sqrt{1-e^2}}{\sin i} K_*. \quad (1)$$

The modified equilibrium temperature T_{eq} is as follows in Eq. 2:

$$T_{eq} = T_{eff} \left(\frac{R_*}{2a} \right)^{1/2}, \quad (2)$$

where T_{eff} is the effective temperature of the host star.

We estimated the relative atmospheric scale height of the atmospheres of our sample using Eq. 3 (Winn et al. 2010);,

$$H = \frac{k_\beta T_{eq}}{\mu_m g_p}, \quad (3)$$

where k_β is Boltzmann’s constant, T_{eq} is the equilibrium temperature of the planet, μ_m the mean molecular mass and g_p the local gravitational acceleration. We adopt a mean molecular mass of approximately 2.3 amu, which is typical for a hot Jupiter exoplanet with a H/He dominated atmosphere (e.g. Sing et al. (2016)). Planets with large atmospheric scale height of many kms are excellent targets for atmospheric characterization through transmission spectroscopy (e.g. Burrows (2014); Mallonn et al. (2015); Sing et al. (2016)).

Moreover, TESS with uninterrupted datasets is expected to improve on the orbital parameters of those systems, hence we can provide a better constrained impact parameter b value for each one of them. The impact parameter is a quantity that shows the projected distance between the planetary center and the stellar center (Seager & Mallén-Ornelas 2003), and it is given by Eq. 4, where i is the inclination of the system and a/R_s is the normalized semi-major axis in units of stellar radii.

$$b = \cos(i) \times a/R_s. \quad (4)$$

5 | RESULTS

We used publicly available datasets from TESS with high-quality photometric precision in order to refine the parameters from ten inflated hot gas giant exoplanets. All the derived parameters from this work for each target are displayed in Tables 3-12, along with their 1σ uncertainty and a reference with their previously obtained parameters. In the following paragraphs, we shortly review each target, including some of their most important features, and present our results with a direct comparison between the individual investigations.

5.1 | WASP-140 b

From the exoplanets observed with TESS and analyzed in this work, the one with the largest radius uncertainty is

WASP-140 b (see Table 1). In the discovery paper (Hellier et al. 2017), WASP-140 b belongs, according to previous observations, to a binary system. WASP-140 A is a K0 star, rather active, with an effective temperature of $T_{\text{eff}}(\text{K}) = 5300 \pm 100$ and $V_{\text{mag}} = 11.1$, while WASP-140 B is about 2 magnitudes fainter. The planet of this system, WASP-140 b, has a mass of $2.4 M_{\text{J}}$ and an orbital period of $P=2.2$ days. It orbits around the host star, WASP-140A, on a grazing, at an impact parameter value $b = 0.93$, and eccentric ($e = 0.047 \pm 0.004$) orbit. WASP-140 b is a massive exoplanet with a short period of a significant eccentricity. All these characteristics of a hot Jupiter are not met usually around K-type stars, and maybe the studies of those are the key indicators to understand the magnetic activity of the host (Poppenhaeger & Wolk 2014). Interestingly, WASP-140 A is considered as a magnetically active star, as there are detected some star-spots on some light curves in the discovery paper. The presence of star-spots on the received light curves are able to alter the correct derivation of the transit depth and the correct measurement of the planetary radius (Morris, Agol, Hebb, & Hawley 2018; Oshagh et al. 2013).

We are interested to investigate this system with TESS and focus on the precise determination of its planetary radius. The large uncertainty of this radius measurement might be attributed to the grazing nature of this system and/or the partial transits reported from ground-based observations. The activity of the host cannot be ruled out, either, as a contributor to this radius uncertainty value.

TESS observed WASP-140 b during the sectors 4, 5 and 31. A total of 28 available light curves were employed in this work to derive the properties of WASP-140 b. Since, WASP-140 system is a known binary with TESS Input Catalog (TIC) identifiers for both stars, the SPOC pipeline estimates a dilution factor and corrects for the amount of the light contamination in the final light curve (Thompson, Fraquelli, Van Cleve, & Caldwell 2016). This dilution metric is named "CROWDSAP" and it is presented on the header of the TESS target pixel files (TPFs). For WASP-140 b, we obtain an average of 0.85 as a crowding estimation, for all the sectors of observation. This value signifies that the contamination of the received flux by nearby sources, is approximately 14%. According to Guerrero et al. (2021), "CROWDSAP" values of less than 0.8 are not trustworthy regarding photometric measurements, therefore for WASP-140 TESS observations, the resulting light curves can be considered as photometrically reliable, since they are not contaminated severely by the companion.

In Fig. A1, we present the TESS folded light curves of WASP-140 b and the best fit transit model at the upper panel. The derived parameters from the emcee approach are shown on the corner plot, at the lower panel. A direct comparison of

this work with the previously published parameters from Hellier et al. (2017) is in Table 3. We pinpoint that our results do not match the previous investigation within 1σ . We report a later mid-time point of 1.2 minutes, while the updated orbital parameters yield a more precise impact parameter value. Even though, the orbital parameters, i and a/R_s , are not in agreement either with the previous results, the uninterrupted TESS data, yielded a better acquisition of those measurements. The high-cadence datasets provided better constrained and more precise i and a/R_s values, which in turn yielded a more precise b for this system of 0.85. However, this newly derived determination of b is associated with a better determination of the transit depth, which now is greatly improved. Moreover, we report a refined measurement of a smaller planetary radius for WASP-140 b by approximately 12%. We also derived a better precision on the reported asymmetric radius uncertainty of WASP-140 b by approximately 86% and 67%. The uncertainty on the planetary radius has been greatly improved by this investigation and places the planet with conviction to a lower inflated radii regime with a smaller estimated temperature. However, the planet remains well beyond the cutoff temperature of 1000K for the inflation to happen (Miller & Fortney 2011), and it continues to have an excess in its radius compatible with its temperature levels.

Exoplanets of grazing transits around moderately bright hosts are difficult to parameterize from the ground, as in the case of WASP-168 b in Hellier et al. (2019). Nevertheless, in this work, using TESS, we improved significantly on the parameters of WASP-140 b, that now it is characterized as a less puffy and more dense exoplanet than it was thought to be.

5.2 | WASP-136 b

Previous studies on WASP-136 b, have shown that this exoplanet belongs to an interesting category of planets, as a short-period hot Jupiter that orbits a sub-giant star. The limited candidates of this population might be attributed to tidal disruption that causes planets to spiral inwards and to the star (Lam et al. 2017).

WASP-136 b completes a full orbit around its evolved late-F host star ($V_{\text{mag}} = 9.93$) in 5.22 days and, with a radius of $1.38 \pm 0.16 R_{\text{J}}$ and mass of $1.51 \pm 0.08 M_{\text{J}}$, it is an inflated giant planet, which is half as dense as Jupiter. Intriguingly, WASP-136 is at its final main sequence phase and the derived planetary radius in the work of Lam et al. (2017) found to be 25% larger than expected in the models of Fortney, Marley, & Barnes (2007). One plausible explanation is that the star moves towards the sub-giant branch and the intensity from the irradiation on the planet is expected to increase dramatically, the planet can heat up, through the stellar irradiation trapped in the interior of the planet, and trigger another re-inflation. A

TABLE 3 Physical properties of WASP-140 b as derived in this work from the modeling of the TESS light curves and the emcee analysis , in comparison to the previously published work of Hellier et al. (2017).

Parameters [units]	This work	Hellier et al. (2017)
	Values $\pm 1\sigma$	Values $\pm 1\sigma$
T_c [BJD _{TDB}]	2456912.35261 \pm 0.00016	2456912.35183* \pm 0.00015
i [°]	84.30 \pm 0.06	83.3 ^{+0.5} _{-0.8}
a/R_s	8.58 \pm 0.06	7.98 \pm 0.39
R_p/R_s	0.1464 \pm 0.0010	0.1656** ^{+0.0494} _{-0.0216}
b	0.851 \pm 0.011	0.93 ^{+0.07} _{-0.03}
R_p [R_J]	1.27 \pm 0.06	1.44 ^{+0.42} _{-0.18}
ρ_p [ρ_J]	1.19 \pm 0.17	0.8 \pm 0.4
$\log g_p$ [cgs]	3.592 \pm 0.009	3.4 \pm 0.2
T_{eq} [K]	1270 \pm 25	1320 \pm 40
H [km]	123 \pm 4	-

* Converted from Heliocentric Julian Date (HJD) of 2456912.35105 \pm 0.00015 to BJD_{TDB}

** From the quoted R_p and R_s values; R_p was poorly constrained since the fitted b makes the transit grazing.

precise radius estimation might provide further clarifications on what the current status of this exoplanet's radius extension is.

We made use of six full transits of WASP-136 b, from the publicly available TESS 2-minutes cadence data in order to update/confirm the previous findings from the discovery paper (Lam et al. 2017), where one full and two partial transits were analyzed. We did not take into consideration the last transit light curve of sector 42, due to a starspot crossing throughout the transit chord that would lead to a biased measurement of the transit depth.

The final modeled light curve with the associated residuals are presented at the upper panel in Fig. A2 , while the best fit parameters are shown in the corner plot at the lower panel. A comparison of the findings in this work with the previous complete study of Lam et al. (2017) is presented in Table 4. The derived R_p/R_s varies significantly from the previous reported value by more than 3σ , indicating deeper transit light curves and larger planetary radius. However, the derived planetary radius is in agreement with the previously reported value, overall. We find an additional difference of 9% in the radius measurement between the two investigations, that makes it a total of 34% larger than expected in Fortney et al. (2007). The uncertainty on the planetary radius of this exoplanet has only been improved marginally with the analysis of the TESS data. We conclude to a larger planetary radius that yields a slightly more inflated and less dense exoplanet, that is consistent with the previous work of Lam et al. (2017).

5.3 | WASP-113 b

WASP-113 b is a hot Jupiter that orbits a G1 type host star in a period of about 4.5 days. In the work of Barros et al. (2016), it is shown that the planet has a mass of $M_p = 0.48 M_J$ and an inflated radius of $R_p = 1.41 R_J$, hence a density of about $\rho_p = 0.172 \rho_J$. However, the planetary radius was expected about 2σ smaller in the work of Fortney et al. (2007), assuming a coreless model. In our work, using TESS, we can confirm/refine the radius measurement of WASP-113 b, and investigate if we can improve on its radius uncertainty.

For this purpose, we analyzed a total of eight transit events (one partial transit was rejected), as they were observed with TESS during sectors 23 and 24. The best-fit model is shown on the upper panel in Fig. A3 , while the best fit parameters are depicted on the corner plot at the lower panel, along with the values of the detrending coefficients. In Table 5, we present the comparison of the newly derived parameters with the previous work of Barros et al. (2016). The radius measurement is in agreement between the two independent investigations, along with the rest of the parameters that were confirmed now with independent datasets provided by TESS. Even though, the TESS data analysis improved only marginally the orbital parameters of this system, however it confirmed an exoplanet of a largely extended atmosphere ($H > 1000$ Km) that orbits a bright host star, i.e., an excellent target for transmission spectroscopy investigations. This is one of the cases where ground-based observations and space-based ones, came into a complete agreement, highlighting this way the good function of the ground- and space-synergy.

TABLE 4 Physical properties of WASP-136 b derived in this work with TESS data, in comparison to the previously published work of Lam et al. (2017).

Parameters [units]	This work	Lam et al. (2017)
	Values $\pm 1\sigma$	Values $\pm 1\sigma$
T_c [BJD _{TDB}]	2456776.9055 ± 0.0011	2456776.90615 ± 0.0011
i [°]	87.7 ± 1.2	$84.7^{+1.6}_{-1.3}$
a/R_s	7.4 ± 0.3	6.43 ± 0.65
R_p/R_s	0.0680 ± 0.0005	0.0641 ± 0.0012
b	0.30 ± 0.16	$0.59^{+0.08}_{-0.14}$
R_p [R_J]	1.50 ± 0.15	1.38 ± 0.16
ρ_p [ρ_J]	0.44 ± 0.14	$0.58^{+0.23}_{-0.15}$
$\log g_p$ [cgs]	3.29 ± 0.05	3.26 ± 0.09
T_{eq} [K]	1630 ± 40	1742 ± 82
H [km]	310 ± 40	-

TABLE 5 Physical properties of WASP-113 b derived in this work from TESS data, in comparison to the previously published work of Barros et al. (2016).

Parameters [units]	This work	Barros et al. (2016)
	Values $\pm 1\sigma$	Values $\pm 1\sigma$
T_c [BJD _{TDB}]	$2457197.09751 \pm 0.00045$	$2457197.098226^* \pm 0.000040$
i [°]	$86.9^{+1.4}_{-1.0}$	$86.46^{+1.2}_{-0.64}$
a/R_s	$8.2^{+0.6}_{-0.5}$	7.87 ± 0.59
R_p/R_s	$0.0917^{+0.0014}_{-0.0013}$	0.0899 ± 0.0015
b	0.45 ± 0.20	$0.486^{+0.063}_{-0.14}$
R_p [R_J]	1.47 ± 0.11	$1.409^{+0.095}_{-0.14}$
ρ_p [ρ_J]	0.15 ± 0.04	$0.172^{+0.055}_{-0.034}$
$\log g_p$ [cgs]	2.73 ± 0.08	$2.744^{+0.081}_{-0.072}$
T_{eq} [K]	1460 ± 70	1496 ± 60
H [km]	1030 ± 230	-

* Converted from HJD of $2457197.097459 \pm 0.00004$ to BJD_{TDB}

5.4 | WASP-120 b

WASP-120 b was discovered and characterized with the work of O. D. Turner et al. (2016). Five ground-based transit observations were used to determine the system's parameters, which yielded a massive exoplanet of $M_p = 4.85 M_J$ and an inflated radius of $R_p = 1.73 R_J$. The eccentricity of WASP-120 b is significant and equal to $e = 0.059 \pm 0.02$. Moreover, this exoplanet has an orbital period of 3.6 days, around its F5 type host. The host star is bright with $V_{mag} = 11$, an age of 0.7 Gyr and rather important activity (O. D. Turner et al. 2016). This activity was pinpointed due to an observed difference, of $1.2 \pm 0.4 \times 10^{-3}$, between the transit depths of two light curves. Another explanation for this difference could

be the presence of a nearby companion. Interestingly, in the work of Bohn et al. (2020), there are hints that the host star belongs to a hierarchical triple system.

TESS revisited this system with four observing sectors. In our work, we employed 24 transit light curves of WASP-120 b, in total. We analyzed the TESS data as for the previous targets of our sample, and we kept the significant eccentricity of this planet as a fixed parameter during the transit light curve fit process. Our results have shown a smaller planetary radius of $R_p = 1.39 \pm 0.08 R_J$ for WASP-120 b, in agreement with the previously published value at 1σ . Also, we report an earlier mid-time transit point by 2.3 minutes, and considering that WASP-120 b is the heaviest exoplanet of our sample, this might be an evidence that transit timing variations

(TTVs) effects take place in this system. The large mass of the planet and the low metallicity of the host star indicate that the planet received a large portion of radiation from its host in order to puff-up and extend its radius. However, WASP-120 was reported to obtain significant activity in O. D. Turner et al. (2016) or, possibly, a companion star. The reported difference between two transit depths of independent observations is confirmed in our work with the analysis of the TESS datasets. More precisely, we fit the 24 light curves individually, with the same emcee process which is based on a MCMC approach, as for the rest of our targets, and obtained the fit transit depths for each of the 24 transit light curves of WASP-120 b. The largest transit depth difference occurs between the transits at the mid-time points of $2458426.172325 \text{ BJD}_{\text{TDB}}$ and $2458447.839933 \text{ BJD}_{\text{TDB}}$, at the observations of sector 4 and sector 5, respectively, and it is approximately $1.1 \pm 0.5 \times 10^{-3}$. We demonstrated that this difference between transit events is repeated and can be attributed to the stellar activity, in agreement with the previous investigation by O. D. Turner et al. (2016). Moreover, we can exclude significant contamination of the datasets due to a companion star by examining the crowding metric, "CROWDSAP", for all the observing sectors. This metric indicates that on average, for all the four sectors of this observation, only 4% of the received light has been obtained from nearby sources. By inspection of the TPF for this exoplanet from TESS, we observed that the companion falls in the detector's field-of-view, hence the SPOC team took this third light contamination into account in the derivation of the PDCSAP flux. This amount of contamination of 4% can be considered in practice negligible as the planet-to-star radius ratio would be underestimated only by 0.02%, hence the aforementioned transit depth difference might be attributed to the host activity and not to the presence of the nearby companion.

Furthermore, with the analysis of the TESS data, we improved the precision of the orbital parameters of this system significantly. The i and a/R_s are not in agreement with the previous work of O. D. Turner et al. (2016), for more than 2σ . Our analysis yielded an updated impact parameter for this system that differs from the previous one for almost 3σ . The larger semi major axis, as derived from the fit, supports the presence of a smaller equilibrium temperature, that deviates from the literature value by approximately 3σ , which consequently yields a reduced atmospheric scale height equal to half its initial value. In Fig. A4, the final model fit is presented. The parameterization of the system after the emcee process and fit is shown on a corner plot at the lower part of the same figure, while a comparison with the work of O. D. Turner et al. (2016), is presented in Table 6. We conclude to a slightly smaller, denser and with a thin atmosphere of less than $H = 100 \text{ km}$ exoplanet.

5.5 | WASP-93 b

WASP-93 b was discovered and characterized in the work of Hay et al. (2016). WASP-93 b has a mass of $M_p = 1.47 M_J$ and it orbits a F4 star with period of about 2.73 days. Later on, in Gajdoš et al. (2019), the estimated radius of WASP-93 b was much smaller than the value published by Hay et al. (2016), $R_p = 0.0873 \pm 0.0025 R_s$ and $R_p = 0.1080 \pm 0.0059 R_s$, respectively. This inconsistency of more than 3σ regarding the planetary radii gave us additional motivation to revisit WASP-93 system and re-evaluate this transit depth measurement with TESS. Therefore, we made use of TESS light curves to compare the findings with this previous estimation, one of which is based on only one transit event (Gajdoš et al. 2019). We used TESS observations of sector 17 in order to revisit and refine the parameters of WASP-93 b. Grazing systems are hard to parameterize due to the fact that their transit light curves have rounded bottoms, constraining this way the information on the orbital parameters derived from a well-defined ingress and egress (when the planet starts to cross the projection of the stellar disk and when it exits). The planetary radii are sometimes poorly defined in grazing systems, but we expect TESS to provide insights on this domain.

For WASP-93 b, in total, there were employed six light curves, cleaned from outliers and detrended from systematics. We analyzed them similarly to our other targets of this investigation. In Fig. A5, we present the best-fit model on the folded light curves on the upper panel. In Hay et al. (2016), it is pinpointed that the mid-times are not well-defined due to uncertainties in the transit ephemeris. Hence, we used in our analysis the revised ephemeris in Gajdoš et al. (2019) ($T_c = 2456079.553552 \pm 0.00457 \text{ BJD}_{\text{TDB}}$). We observed an offset in our transits' ingress of approximately 9.3 minutes later. The almost v-shaped transit gives indications of a background star that might contribute significantly to the received light curve. However, there are no companions with important brightness in the proximity in order to produce such effect, while another scenario could be that WASP-93 b belongs to a triple system (Hay et al. 2016). The final parameters of the system are shown at the corner plot in Fig. A5, while the comparison with the works of Hay et al. (2016) and Gajdoš et al. (2019) are presented in Table 7. The planetary radius of $R_p = 1.54 \pm 0.06 R_J$ derived in our work is consistent with the work of Hay et al. (2016) of $R_p = 1.597 \pm 0.077 R_J$, within 1σ . The derived parameters agree broadly with the published ones, while the transit depth and planetary radius are significantly different from in the work of Gajdoš et al. (2019) with $R_p/R_s = 0.0873 \pm 0.0025$ and $R_p = 1.29 \pm 0.05 R_J$. This TESS investigation improved only marginally on the planetary radius uncertainty, it confirmed the findings in Hay et al. (2016) and solved a discrepancy between the two reported

TABLE 6 Physical properties of WASP-120 b derived in this work with TESS data, in comparison to the previously published work of O. D. Turner et al. (2016).

Parameters[units]	This work	O. D. Turner et al. (2016)
	Values $\pm 1\sigma$	Values $\pm 1\sigma$
T_c [BJD _{TDB}]	2456779.4347 \pm 0.0005	2456779.4363* \pm 0.0005
i [°]	84.54 \pm 0.35	82.54 \pm 0.78
a/R_s	6.8 \pm 0.2	5.90 \pm 0.339
R_p/R_s	0.0751 \pm 0.0005	0.08093 \pm 0.00099**
b	0.65 \pm 0.05	0.78 \pm 0.02
R_p [R_J]	1.39 \pm 0.08	1.473 \pm 0.096
ρ_p [ρ_J]	1.76 \pm 0.32	1.51 ^{+0.33} _{-0.26}
$\log g_p$ [cgs]	3.86 \pm 0.03	3.707 \pm 0.056
T_{eq} [K]	1749 \pm 41	1880 \pm 70
H [km]	90 \pm 7	-

* Converted from HJD of 2456779.43556 \pm 0.00051 to BJD_{TDB}

** Computed from the given $(R_p/R_s)^2 = 0.00655 \pm 0.00016$

transit depths for WASP-93 b. Interestingly, the orbital parameters are consistent within 1σ , supporting a grazing exoplanet in all of these works, highlighting the need to parameterize grazing systems with caution. In a recent work published by Wong et al. (2021), the planetary radius and orbital parameters are in complete agreement with our work.

5.6 | HAT-P-16 b

HAT-P-16 b is a transiting inflated hot Jupiter exoplanet that orbits a bright F8 dwarf ($V_{mag} = 10.8$) every 2.77 days on an eccentric orbit ($e = 0.036$). This is the second heaviest exoplanet of our sample. From previous investigations on this exoplanet (Buchhave et al. 2010), the planetary radius is estimated as $R_p = 1.289 \pm 0.066 R_J$, its planetary mass as $M_p = 4.193 \pm 0.094 M_J$ and its density $\rho_p = 2.42 \pm 0.35 \text{ g cm}^{-3}$.

Using seven light curves obtained with TESS, we revisited this system and defined its properties. We kept the eccentricity (as with the previously highly eccentric systems) fixed to the literature value during the transit light curve fit process. The best fit transit model is shown at the top panel of Fig. A6, and the associated best fit parameter corner plot on the lower panel of that same figure. At Table 8, we present the comparison of our work with the investigations by Buchhave et al. (2010) and Ciceri et al. (2013). With the analysis of the TESS datasets, we report a later transit by 15 minutes for HAT-P-16 b, an indication that probable TTVs are present. Since it is a massive exoplanet, TTVs are not unusual in this case. The derived orbital parameters are in a broad agreement with the works of Ciceri et al. (2013) and Buchhave et al. (2010), while the impact parameter is consistent within 1σ with the work of

Ciceri et al. (2013). The newly derived planetary radius is in better agreement with the work of Buchhave et al. (2010), within 1σ . Even though, with our TESS investigation we did not improve on the planetary radius uncertainty of this system, however we confirmed a planet with the same density and surface gravity as thought in Buchhave et al. (2010). In the future, TESS is not expected to observe HAT-P-16 b again.

5.7 | WASP-123 b

WASP-123 b orbits a bright ($V_{mag} = 11.1$) G5 star, every 3 days. It is a hot Jupiter with an inflated radius of $R_p = 1.32 R_J$. Considering the measurement of its mass of $M_p = 0.9 M_J$, the planet has a density of about $\rho_p = 0.4 \rho_J$ (O. D. Turner et al. 2016). It is a rather typical hot Jupiter and the revision of its planetary radius will contribute to the understanding of the general picture of this kind of exoplanets around evolved stars.

The analysis of the TESS datasets based on observations on this exoplanet from the sectors 13 and 27, interestingly, showed that there is a discrepancy regarding the derived transit depths. In sector 13, we derived an $R_p/R_s = 0.1240 \pm 0.0012$, while in sector 27, $R_p/R_s = 0.1054 \pm 0.0008$. To investigate this case, we made use of the "CROWDSAP" metric, that defines the ratio between the target flux and the total flux that falls on the photometric aperture. The PDCSAP fluxes are usually adjusted according to this crowding factor. For WASP-123 b observations at sector 13, the CROWDSAP metric is about 69.3%, while for sector 27, it is 89.8% and this indicates, for sector 13, a contamination due to third light of approximately 30%, while for sector 27, of about 10%. In Guerrero et al. (2021), it is pinpointed that "CROWDSAP"

TABLE 7 Physical properties of WASP-93 b derived in this work with TESS data, in comparison to the previously published works of Hay et al. (2016) and Gajdoš et al. (2019).

Parameters [units]	This work	Hay et al. (2016)	Gajdoš et al. (2019)
	Values $\pm 1\sigma$	Values $\pm 1\sigma$	Values $\pm 1\sigma$
T_c [BJD _{TDB}]	2456079.560 \pm 0.0046	2456079.5650* \pm 0.0004	2456079.553552* \pm 0.00457
i [°]	81.55 \pm 0.32	81.18 \pm 0.29	82.27 \pm 0.58
a/R_s	6.11 ^{+0.18} _{-0.15}	5.94 \pm 0.13	6.45 \pm 0.35
R_p/R_s	0.1017 ^{+0.0028} _{-0.0020}	0.10474 \pm 0.00062**	0.0873 \pm 0.0025
b	0.90 \pm 0.04	0.904 \pm 0.009	0.868 \pm 0.080
R_p [R_J]	1.54 \pm 0.06	1.597 \pm 0.077	1.29 \pm 0.05***
ρ_p [ρ_J]	0.40 \pm 0.09	0.360 \pm 0.084	-
$\log g_p$ [cgs]	3.17 \pm 0.09	3.120 \pm 0.093	-
T_{eq} [K]	1910 \pm 40	1942 \pm 38	-
H [km]	480 \pm 110	-	-

* Converted to BJD_{TDB} from 2456079.56420 \pm 0.00045 and 2456079.55280 \pm 0.00457 HJD (Gajdoš et al. 2019).

** Computed from the given $(R_p/R_s)^2 = 0.01097 \pm 0.00013$

***From the quoted R_p estimation in units of Earth radii provided in that work.

TABLE 8 Parameter refinement of HAT-P-16 b using high-cadence TESS data. The R_p value as derived from the analysis in our work is in better agreement with Buchhave et al. (2010) within 1σ significance.

Parameters [units]	This work	Buchhave et al. (2010)	Ciceri et al. (2013)
	Values $\pm 1\sigma$	Values $\pm 1\sigma$	Values $\pm 1\sigma$
T_c [BJD _{TDB}]	2455027.60356 \pm 0.00035	2455027.59293 \pm 0.00031	2455027.59281 \pm 0.00040
i [°]	88.4 \pm 1.0	86.6 \pm 0.7	87.74 \pm 0.59
a/R_s	7.73 \pm 0.23	7.17 \pm 0.28	7.67 \pm 0.18*
R_p/R_s	0.1063 \pm 0.0007	0.1071 \pm 0.0014	0.1067 \pm 0.0014
b	0.220 \pm 0.130	0.439 ^{+0.065} _{-0.098}	0.30 \pm 0.08*
R_p [R_J]	1.31 \pm 0.06	1.289 \pm 0.066	1.190 \pm 0.035
ρ_p [ρ_J]	1.87 \pm 0.25	1.95 \pm 0.28**	2.33 \pm 0.20
$\log g_p$ [cgs]	3.804 \pm 0.027	3.8 \pm 0.04	3.87 \pm 0.024
T_{eq} [K]	1566 \pm 31	1626 \pm 40	1567 \pm 22
H [km]	93 \pm 7	-	-

* Estimated from the given values for the angular separation of the system in AU and for the inclination in Ciceri et al. (2013).

** Converted to units of Jupiter's density from $\rho_p = 2.42 \pm 0.35 \text{ g cm}^{-3}$ (Buchhave et al. 2010).

values of less than 0.8 yield an unreliable photometry. However, this metric can be sometimes underestimated by the PDC pipeline and can yield an overestimated third light contamination, as in the work of Parviainen et al. (2021) for the exoplanet TOI-519 b. Sector 27 observations support an exoplanet much less contaminated from third sources than sector 13. Based on this, we expect the transits in sector 13 to yield a biased parameter refinement.

We checked the TOI-catalog ⁷, to investigate further this discrepancy and find the reason of its occurrence. As a public comment, it is mentioned that the transits of WASP-123 b affected the star with TIC31858844, for the entire sector observation. In the work of Bohn et al. (2020), the companion to WASP-123 has only a separation of 4.8". It has a stellar mass of 0.4 M_s and effective temperature $T_{\text{eff}}(\text{K}) = 3524$. One

⁷<https://tev.mit.edu/data/>

scenario is that this is highly active M2 dwarf that is blended in the photometry of its companion during the transiting event of WASP-123 b, hence the lower flux that was received in the photometric aperture from WASP-123. We neglected the transits of sector 13, since we cannot account for the missing light, and in our analysis we used only the data from sector 27, which contains transit observations with better target focused photometry. The TIC number of the stellar companion is registered in the TOI-catalog, indicating that the crowding factor is taken into account for the correction of the final PDCSAP light curve.

In total, we employed seven light curves for our analysis. The best model fit is shown at the upper left panel in Fig. A7 (while the best fit model from sector 13 investigation is presented on the right panel for comparison), and the final parameters are presented at the corner plot at the lower panel of the same figure. The comparison with the previous work of O. D. Turner et al. (2016) is shown in Table 9. Our TESS findings, other than a later transit midpoint by 2.3 minutes, are completely consistent with this previous work, even though they did not show any significant improvement on the uncertainty on the planetary radius of this exoplanet either.

5.8 | WASP-76 b

WASP-76 b was discovered and characterized with the work of West et al. (2016). This exoplanet is an inflated hot Jupiter ($R_p = 1.83 R_J$) that orbits its bright ($V_{mag} = 9.5$) F7 host in 1.8 days. In the recent work of Southworth, Bohn, Kenworthy, Ginski, & Mancini (2020), the authors wanted to account for the partial transits of the discovery paper that they were highly contaminated with red noise, and they proceeded with a refinement of this system using one full transit light curve of WASP-76 b obtained from CAHA 1.23m. The authors have discovered that the transit occurred 8.6 minutes earlier than predicted and the orbital period was 0.54s shorter than the expected value. Hence, it is suggested that TTVs might be responsible for this deviation. Moreover, they reported a larger radius ($R_p/R_J = 1.885_{-0.042}^{+0.117}$) and a higher equilibrium temperature ($T_{eq} = 2235_{-23}^{+56}$) in comparison to the discovery paper.

During the previous years, numerous studies were conducted on this exoplanet, interestingly some of them using large ground-based telescopes such as the Very Large Telescope (VLT) (Ehrenreich et al. 2020) and/or space telescopes such as the Hubble Space Telescope (HST) (von Essen et al. 2020). Observations with TESS are currently available to contribute to the understanding of the WASP-76 b planetary system. For this purpose, we made use of TESS observations during sectors 30 and 42. In total, 23 light curves were employed in our analysis. Interestingly, we derived a new

transit mid-time, as a free parameter from our MCMC analysis, using emcee, and it appears to occur approximately 14 minutes earlier than expected from West et al. (2016), while the orbital period is found to agree with Southworth et al. (2020) and be 0.47s shorter. We, therefore, confirm the need for a TTV analysis for this system. Moreover, even though our analysis did not improve on the planetary radius uncertainty of this exoplanet either, the high photometric quality of TESS yielded a planetary radius of $1.83 \pm 0.04 R_J$, which is in complete agreement with West et al. (2016). However, the analysis in order to derive the transit depth in West et al. (2016) neglects completely the contribution of WASP-76A's companion. WASP-76B has a $0.4438''$ separation, and it is 2.58 times fainter than WASP-76A. The flux contrast between the two stars is approximately 10 (Ehrenreich et al. 2020). Using Eq. 5 in Ciardi, Beichman, Horch, & Howell (2015), we applied a correction factor of $\sqrt{1.1}$ to our transit depth, which is compatible with the value of 1.4 that it is suggested in Ciardi et al. (2015), as a typical factor to apply, to account for the contamination of the third light when the planet transits the primary (instead of the secondary) star. This correction yielded a new $R_p/R_s = 0.111425 \pm 0.000094$, and moreover a new planetary radius of $R_p = 1.92 \pm 0.04$, which is in complete agreement with the latest works on this subject (Ehrenreich et al. 2020; Southworth et al. 2020; von Essen et al. 2020). The corrected planetary radius yields also a new density estimation of $\rho_p = 0.13 \pm 0.01$ (consequently more parameters are affected by this change in radius and density, and yield a $\log g_p = 2.750 \pm 0.007$, and a $H = 1471 \pm 34$), which is in agreement with the previous within 2σ , and suggests now a less dense exoplanet. This TESS analysis confirmed the latest reports on this exoplanet, however it also provided a valuable precision in R_p/R_s , in comparison to all the other works, which is very useful for transmission spectroscopy investigations. Regarding the TESS light curve of this target, and the crowding metric being "CROWDSAP" = 0.99972, this signifies that only the 0.3% of this PDCSAP flux comes from contaminating sources. In this case, the analysis of the TESS light curves support the work of Ehrenreich et al. (2020) where they did not confirm the companion either, or, as they suggest, it is completely hiding behind WASP-76A and does not contribute in the received photometry significantly. It is worthy noting that WASP-76B is not registered with an allocated TIC number, which might be a reason why the SPOC team did not consider a dilution factor for this system. In Fig. A8, we present at the upper panel, the final fit of the TESS light curves along with the associated residuals, while at the lower panel, we present the derived values from the emcee process. We pinpoint here that our work is in a direct comparison to West et al. (2016), where the authors did not account for the third light contribution, since at the TESS datasets, the companion

TABLE 9 Physical properties of WASP-123 b derived in this work with TESS data solely from Sector 27 (see in text), in comparison to the previously published work of O. D. Turner et al. (2016).

Parameters[units]	This work	O. D. Turner et al. (2016)
	Values $\pm 1\sigma$	Values $\pm 1\sigma$
T_c [BJD _{TDB}]	2456845.1735 ± 0.0004	$2456845.171610 \pm 0.00039$ *
i [°]	86.2 ± 0.5	85.74 ± 0.55
a/R_s	7.29 ± 0.20	7.13 ± 0.25
R_p/R_s	0.1053 ± 0.0007	0.10536 ± 0.00128 **
b	0.48 ± 0.06	0.530 ± 0.049
R_p [R_J]	1.35 ± 0.05	1.318 ± 0.065
ρ_p [ρ_J]	0.37 ± 0.05	0.393 ± 0.056
$\log g_p$ [cgs]	3.063 ± 0.026	3.07 ± 0.04
T_{eq} [K]	1500 ± 40	1520 ± 50
H [km]	490 ± 40	–

* Converted in BJD_{TDB} from $2456845.17082 \pm 0.00039$ HJD in O. D. Turner et al. (2016).

** Computed from the given $(R_p/R_s)^2 = 0.01110 \pm 0.00027$ in O. D. Turner et al. (2016).

is not taken under consideration either, or its contribution is not significant, as it appears from the value of the crowding metric.

5.9 | WASP-20 b

WASP-20 b was discovered and characterized in the work of Anderson et al. (2015). The binarity of this system (companion at $0.26''$) was analyzed in the work of Evans, Southworth, & Smalley (2016), where three scenarios were considered. WASP-20 b is an inflated, Saturn-mass planet. If we ignore the binarity of the system, the planetary radius and planetary mass are $R_p = 1.20 \pm 0.14 R_J$ and $M_p = 0.291 \pm 0.017 M_J$, if the planet transits the brighter star of this system then $R_p = 1.28 \pm 0.15 R_J$ and $M_p = 0.378 \pm 0.022 M_J$ and if the planet orbits the fainter star then $R_p = 1.69 \pm 0.12 R_J$ and $M_p = 1.30 \pm 0.19 M_J$. With TESS, we revisited this interesting system. Using two sectors of TESS observations and a total of ten light curves, we refined the planetary radius to $R_p = 1.38 \pm 0.04 R_J$. Recently, Southworth et al. (2020) tried to determine the planetary radius of WASP-20 b with TESS observations of sector 2. They concluded to $R_p = 1.382 \pm 0.057 R_J$ for a transit around the brighter star and $R_p = 1.69 \pm 0.11 R_J$ for a transit around the fainter star. We used TESS observations of all the available sectors, sector 2 and sector 29, to eventually confirm those findings. The best fit model is shown in Fig. A9, at the upper panel therein, and the final parameterization appears on the corner plot at the lower panel. The comparison with the previous work that yielded a full parameterization of the system (Anderson et al. 2015) is presented in the Table 11.

In TESS observations the companion star is not identified with a TIC number, hence the "CROWDSAP" metric of, an average from both sectors, of 0.997, might not take into account the third light contribution from WASP-20B. Therefore, to account for this contamination of 3%, we used the correction factor of 1.34, as in Southworth et al. (2020) for the analysis of the TESS data of sector 2. We adopted the stellar radius of the work of Southworth et al. (2020) of $R_s = 1.242 \pm 0.044 R_\odot$ and with a derived $R_p/R_s = 0.1153 \pm 0.0005$, which agrees within 1σ with the previous work on TESS data, we concluded to a planetary radius of $R_p = 1.43 \pm 0.05 R_J$. This planetary radius is in good agreement with both previous works of Anderson et al. (2015) and Southworth et al. (2020). However, the stellar radii considered in those works are much different with $R_s = 1.392 \pm 0.044 R_\odot$ and $R_s = 1.242 \pm 0.044 R_\odot$ respectively. Taken into account the stellar radius derived in the ground based investigation instead, we concluded to a planetary radius of $1.6 R_J$. This is another example of the necessity of the correct parameterization of the stellar parameters in order to obtain accurate planetary parameters. For this same system, furthermore, we report a later transit, by approximately 13.7 minutes, hence TTVs might be present, even though it is unlikely considering the small mass of the planet. The derived planetary radius is in agreement with Anderson et al. (2015), and also consistent with the "planet transits star A" scenario in Southworth et al. (2020). The planetary radius uncertainty is confirmed as well with the TESS independent space observations and the orbital parameters are verified too. Overall, TESS confirmed an inflated giant with many

TABLE 10 Physical properties of WASP-76 b, as derived in this work with TESS data, in comparison to the previously published work of West et al. (2016). In brackets, we present the derived values considering the third light contamination.

Parameters[units]	This work - [L3 correction]	West et al. (2016)
	Values $\pm 1\sigma$	Values $\pm 1\sigma$
T_c [BJD _{TDB}]	2456107.84623 \pm 0.00030	2456107.855819* \pm 0.00034
i [$^\circ$]	89.4 ^{+0.5} _{-0.6}	88.0 ^{+1.3} _{-1.6}
a/R_s	4.1 \pm 0.01	4.102 \pm 0.062
R_p/R_s	0.10624 \pm 0.00009 – [0.111425 \pm 0.000094]	0.10630** \pm 0.0035
b	0.04 \pm 0.05	0.14 ^{+0.11} _{-0.09}
R_p [R_J]	1.83 \pm 0.04 – [1.92 \pm 0.04]	1.83 ^{+0.06} _{-0.04}
ρ_p [ρ_J]	0.15 \pm 0.01 – [0.13 \pm 0.01]	0.151 \pm 0.010
$\log g_p$ [cgs]	2.791 \pm 0.007 – [2.750 \pm 0.007]	2.80 \pm 0.02
T_{eq} [K]	2182 \pm 35	2160 \pm 40
H [km]	1335 \pm 31 – [1471 \pm 34]	-

* Converted from 2456107.85507 \pm 0.00034 HJD.

**Estimated from the quoted R_p and R_s values in West et al. (2016).

kms of atmospheric scale height, suitable for transmission spectroscopy investigations.

with the previously derived values of Anderson et al. (2014) is shown in Table 12.

5.10 | WASP-108 b

WASP-108 b was discovered and characterized in the work of Anderson et al. (2014). The authors presented a bloated hot Jupiter of an inflated radius of $1.284 \pm 0.047 R_J$ which orbits a relatively bright ($V_{mag} = 11.2$) F9 star on a 2.68-days period. Recently, a companion star to WASP-108 was reported in the work of Bohn et al. (2020).

Even though, this previous work of Anderson et al. (2014) appears only in the archive, eventually this planet is confirmed with independent space observations with TESS. Observing sectors 11, 37 and 38, provided a total of 25 transit light curves to analyze. Interestingly, our MCMC process, based on the emcee implementation, yielded a difference in R_p/R_s by more than 3σ . However, the crowding metric indicated that there was a correction of the received light curves for a contamination of approximately 13% by nearby sources, and this can be the main reason for the observed difference in the transit depth between our analysis and the previous work by Anderson et al. (2014). We report also a later transit mid-time by 5.6 minutes, while the orbital parameters are all in agreement with this previous investigation, within 1σ . However, the derived planetary radius is consequently larger, since the third light contamination is taken into account, and supports now a less dense exoplanet scenario for WASP-108 b. The modeled TESS light curve is shown on the upper panel of Fig. A10, while the derived parameters for this exoplanet are shown in the corner plot on the lower part of the figure. A direct comparison

6 | DISCUSSION

In the following paragraphs, we discuss the highlights of our analysis. More specifically, how the R_p (and the uncertainties on their measurements) derived from previous investigations and the measurements of R_p from our TESS analysis can be compared. Furthermore, we compare our newly derived b for these systems to the previously reported b values, and eventually we assess how these two quantities (R_p and b) are related. Better constrained b values, derived from a well acquired information on ingress and egress, place the planet to a more precise orbital configuration around its host. This consequently can yield a more robust R_p value, since the planetary radii are usually vulnerable towards the stellar limb darkening modeling process (Alexoudi et al. 2020).

6.1 | Planetary radius refinement

For each one of the exoplanets of our sample, we derived their planetary radii through the analysis of TESS observations of single and multiple sectors. In Fig. 1, we present the derived planetary radii with their uncertainties. The radii measurements are located approximately on the line of equality for $R_p = R_{p(\text{TESS})}$. However, for WASP-140 b there is a significant decrease in the planetary radius by 12% and its uncertainty is reduced by a factor of 3. This can be attributed to the fact that the transit analysis of the previously published work

TABLE 11 Physical properties of WASP-20 b, as derived in this work with TESS data, in comparison to the previously published work of Anderson et al. (2015). The dataset is in rather complete agreement with the work of Southworth et al. (2020) (see in text). In brackets, we present the derived values considering the third light contamination of the companion star.

Parameters[units]	This work - [L3 correction]	Anderson et al. (2015)
	Values $\pm 1\sigma$	Values $\pm 1\sigma$
T_c [BJD _{TDB}]	2455715.66591 \pm 0.00034	2455715.6564 \pm 0.0003 *
i [°]	85.82 \pm 0.16	85.56 \pm 0.22
a/R_s	9.50 \pm 0.17	9.29 \pm 0.23
R_p/R_s	0.09963 \pm 0.00047 - [0.1153 \pm 0.0005]	0.10775 \pm 0.00102**
b	0.691 \pm 0.028	0.718 \pm 0.018
R_p [R _J]	1.38 \pm 0.04 - [1.43 \pm 0.05]	1.458 \pm 0.057
ρ_p [ρ_J]	0.118 \pm 0.012 - [0.108 \pm 0.013]	0.1006 ^{+0.0131} _{-0.0099}
$\log g_p$ [cgs]	2.585 \pm 0.027 - [2.46 \pm 0.03]	2.527 \pm 0.036
T_{eq} [K]	1362 \pm 26	1379 \pm 32
H [km]	1340 \pm 90 - [1790 \pm 123]	-

* Converted from 2455715.65562 \pm 0.00028 BJD_{UTC}

** Computed from the given $(R_p/R_s)^2 = 0.01161 \pm 0.00022$ in Anderson et al. (2015).

TABLE 12 Physical properties of WASP-108 b, as derived in this work with TESS data, in comparison to the work of Anderson et al. (2014).

Parameters[units]	This work	Anderson et al. (2014)
	Values $\pm 1\sigma$	Values $\pm 1\sigma$
T_c [BJD _{TDB}]	2456413.79490 \pm 0.00018	2456413.79098 \pm 0.00015 *
i [°]	89.2 \pm 0.7	88.49 \pm 0.84
a/R_s	7.03 \pm 0.08	7.05 \pm 0.13
R_p/R_s	0.11165 \pm 0.00029	0.10867 \pm 0.00069 **
b	0.10 \pm 0.09	0.19 \pm 0.10
R_p [R _J]	1.35 \pm 0.04	1.284 \pm 0.047
ρ_p [ρ_J]	0.36 \pm 0.04	0.422 \pm 0.033
$\log g_p$ [cgs]	3.040 \pm 0.017	3.093 \pm 0.023
T_{eq} [K]	1589 \pm 33	1590 \pm 36
H [km]	547 \pm 26	-

* Converted from 2456413.79019 \pm 0.00015 HJD

** Computed from the given $(R_p/R_s)^2 = 0.01181 \pm 0.00015$ in Anderson et al. (2014).

on this exoplanet concluded to a system with larger impact parameter value, hence a more grazing orbit. For the rest of exoplanets of the sample, the planetary radii agree within 1σ with the previous investigations. It is currently investigated by our group if TESS can improve to this extent the radii uncertainty of other exoplanets like WASP-140 b, regarding its grazing orbit around a host star of similar brightness. In our sample, WASP-93 is similar to WASP-140 in terms of a grazing orbit and similar host's apparent magnitude. However, for

WASP-93 b, the radius uncertainty was confirmed by TESS, rather than improved. It is interesting to investigate if TESS can improve on the planetary radii and orbital parameters of similar systems to WASP-140 b, orbiting early K-type host stars. Interestingly, WASP-177 (O. D. Turner et al. 2019) is a K2 type host ($V_{mag} = 12.3$) of a planet with a grazing orbit ($b=0.98$) and will be observed with TESS during sectors 42 and 55. WASP-183 b (O. D. Turner et al. 2019), which belongs also to a grazing system ($b=0.92$), orbits a slightly fainter star

of G9/K0 type with $V_{mag} = 12.76$ and will be observed by TESS during sectors 45 and 46. The photometric investigations of those two candidates might shed light whether there is a window in photometric observations where TESS in practice holds an advantage.

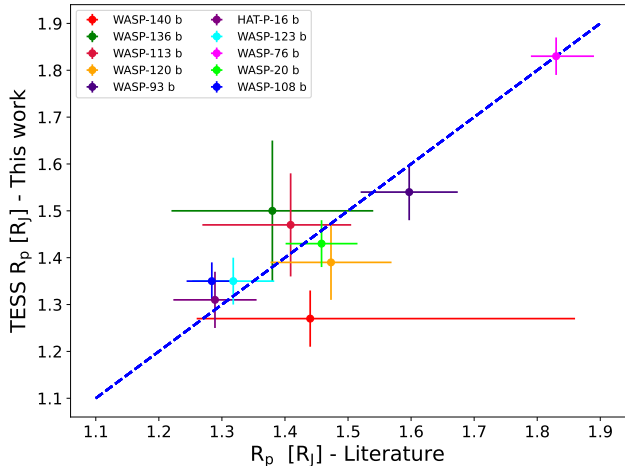


FIGURE 1 The new planetary radii as derived from TESS observations for each one of the exoplanets of our sample, in comparison to the previously published planetary radii values. The uncertainties on the radii are mostly the same within 1σ . The exception is the uncertainty on the radius of WASP-140 b, which has been greatly improved by TESS.

6.2 | Impact Parameter refinement

The analysis of the TESS datasets has shown that for some cases the orbital parameter refinement also resulted in a different impact parameter estimation. In Fig. 2, we present the expected literature value for the impact parameter of each system and the derived TESS value. All the impact parameters derived with TESS are smaller (or equivalent) to the expected ones, likely due to the better continuous photometry provided by TESS. The ingress and egress of each system is monitored in high-quality data, and the orbital parameters i and a/R_s are better constrained. Overall, the TESS b values are in agreement with the previous investigations within 1σ . Except the cases of WASP-140 b, WASP-136 b, WASP-120 b and HAT-P-16 b. For these, i and a/R_s deviate between $1 - 2.5\sigma$ from the previous researches, and this yields a b for these systems that deviates also accordingly. For some systems of our sample, the eccentricity is not negligible. However, the non-zero eccentricity of WASP-140 b ($e = 0.047 \pm 0.004$), WASP-120 b ($e = 0.059 \pm 0.02$) and HAT-P-16 b ($e = 0.036 \pm$

0.004), is expected to play a minor role in the derivation of the impact parameters, based on Eq.7 from Winn et al. (2010).

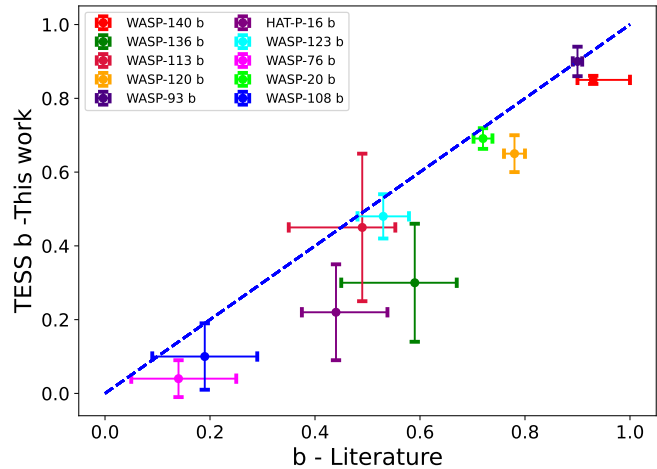


FIGURE 2 Here, we depict a comparison between the b values from the literature, and the b measurements as derived from the analysis of high-cadence TESS data. TESS confirmed b within 2σ significance for all the exoplanets of our sample, except for WASP-120 b. The new b measurement for this exoplanet varies by more than 2σ from the previous estimation, since the TESS analysis refined significantly ($> 2\sigma$) its orbital parameters of i and a/R_s .

6.3 | The relations between the planetary radii and the impact parameters

The derived value of the radius of an exoplanet is strongly affected by the orbital set-up of the system. If the planet is transiting its host star centrally ($b=0$) or over the limbs ($b=1$), this plays a major role in the correct estimation of the transit depth (Alexoudi et al. 2020). As we saw previously, b depends on i and a/R_s . This information on the orbital parameters is usually acquired from a well-defined ingress and egress in the received light curve. For specific ground-based observations that the analysis is solely based on light curves from partial transits or really noisy datasets, this might yield poorly constrained orbital parameters. However, TESS with a 27-days uninterrupted photometry, confirmed b for most of the planets in our sample. For the ones that their orbital parameters were refined within 2σ from the previous investigations.

In the upper panel, in Fig. 3, we present the previous investigations of the R_p and b measurements of these systems in fainter colors, while in vivid colors we depict the results as

derived in this work using TESS. At the lower panel, it is noticeable that for systems of $b > 0.6$ the planetary radii have been overestimated by the previous investigations, while for centrally transiting systems the published radii were slightly underestimated. This is an indication that poorly constrained grazing systems likely yield an overestimation of planetary radii. However, our sample is small to verify this. The importance of this finding is currently under investigation by our team, using a rich sample of grazing systems observed with TESS.

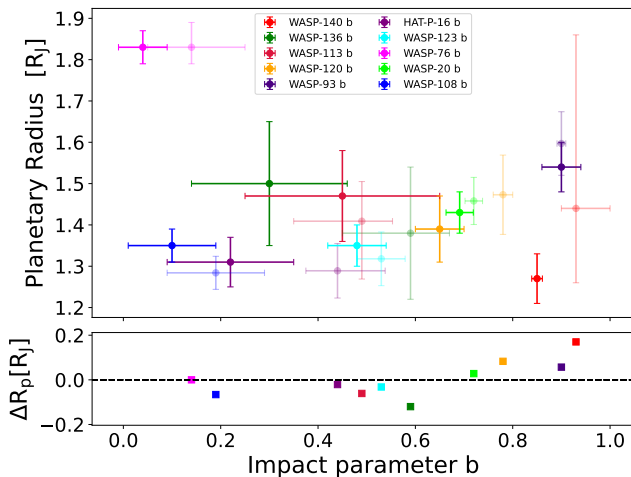


FIGURE 3 In the upper panel, we show the planetary radii derived in this work, in comparison to the impact parameter of these systems. In fainter colors, we present the literature measurements, while in vivid colors we depict the measurements as derived from the analysis of high-cadence TESS data. WASP-140 b, WASP-136 b, WASP-120 b and HAT-P-16 b are not in a complete agreement with the previous investigations. On the lower panel, we present the difference between the planetary radius reported in the literature and the planetary radius derived from TESS observations (colored squares). We plotted this difference versus the literature b value. For $b > 0.6$, the R_p values appear slightly overestimated by the ground-based investigations.

7 | SUMMARY AND CONCLUSIONS

In this work, we employed a small sample of inflated hot giants and using high-quality uninterrupted datasets, provided by TESS, we aimed to improve on their planetary radius uncertainty. For this purpose, we chose exoplanets that have the largest reported uncertainty on their planetary radii, in the

literature. The precise measurement of the planetary radius can help the evolutionary models to predict the presence or the absence of a planetary core and the interior energy of the planet (Bodenheimer, Laughlin, & Lin 2003).

First, we obtained the publicly available transit light curves from each system and then we fit those light curves using a detrending and a transit model. Through a MCMC approach, using emcee, we provided best fit values for each model that was applied on the light curves. Then we used these best fit values to derive the new planetary parameters for each system.

The results have shown that only WASP-140 b was benefited significantly from the TESS investigation with respect to its planetary radius uncertainty. Nevertheless, by using TESS's unprecedented precision, we were able to report the planetary radii refinement/confirmation of a sample of inflated hot giant exoplanets. The high precision of TESS not only yielded refined planetary parameters for WASP-140 b, it also improved the orbital parameters of WASP-120 b. For the latter, the large amount of continuous high-quality data, spread over four sectors of TESS observations, was the reason to derive better constrained orbital parameters for this system. Another outcome of our investigation is the clarification on the discrepancy regarding the planetary radius of WASP-93 b, between the independent investigations in Hay et al. (2016) and Gajdoš et al. (2019). For all the other exoplanets of our sample, the derived parameters are in agreement with the previous investigations (within $1 - 2\sigma$). Last but not least, we report an indication that the ground-based investigations likely have overestimated the R_p value for systems with $b > 0.6$. This needs to be confirmed with the analysis of high-quality TESS datasets of a rich sample of (near-)grazing systems.

For most of the cases, TESS confirmed the previous investigations demonstrating that excellent photometric studies can be achieved with small telescopes of the class of 1m (e.g. 1.2m STELLA⁸ (Strassmeier et al. 2004, 2010) or the 1.23m CAHA⁹), that can reach photometric sensitivity of 1 mmag (e.g. Ciceri et al. (2013); Mallonn et al. (2015)) or even lower in some cases (Mallonn, Poppenhaeager, Granzer, Weber, & Strassmeier 2021). However, the correct parameterization from the ground is sometimes vulnerable, due to the large point-to-point scatter of the data at the transit light curve, or due to incomplete transit datasets that lack the information on ingress and egress. For these investigations, TESS, with uninterrupted (exception is the data downloading time) and high-quality light curves, can contribute as a complementary tool to the ground-based investigations, in order to verify, or to refine the parameters of exoplanetary systems with independent measurements from space. Moreover, TESS

⁸stella.aip.de

⁹www.caha.es/CAHA/Telescopes/1.2m.htm

observations could be combined with ground-based observations delivering high-fidelity datasets. One option is to try to combine TESS's precision with high-quality photometry from ground-based instruments in order to construct a transmission spectrum for atmospheric characterization (Yip et al. 2021). Eventually, future instrumentation (e.g. JWST (Gardner et al. 2006), PLATO (Rauer et al. 2014)) is expected to improve on the exoplanetary parameters tremendously. Till then, TESS will hold the fort by providing photometric data of the highest quality, available to the community for further researches and investigations on exoplanetary systems.

8 | ACKNOWLEDGMENTS

We would like to thank Klaus Strassmeier, Matthias Mallonn, Katja Poppenhaeger, Ekaterina Dineva and Engin Keles, for useful discussions, questions, comments and suggestions that helped to improve this work significantly. We sincerely appreciate the useful comments and suggestions from the anonymous reviewer, which enriched the quality of the manuscript. XA thanks Ioannis Mitsos for fruitful discussions regarding code structure and optimization. This paper includes data collected by the TESS mission, which are publicly available from the Mikulski Archive for Space Telescopes (MAST). Funding for the TESS mission is provided by the NASA Explorer Program. This research made use of Lightkurve, a Python package for Kepler and TESS data analysis (Lightkurve Collaboration, 2018). XA is grateful for the financial support from the Potsdam Graduate School (PoGS) in the form of a doctoral scholarship.

REFERENCES

- Alexoudi, X., Mallonn, M., Keles, E., Poppenhäger, K., von Essen, C., & Strassmeier, K. G. 2020, *A&A*, 640, A134. doi: 10.1051/0004-6361/202038080
- Alexoudi, X., Mallonn, M., von Essen, C. et al. 2018, *A&A*, 620, A142. doi: 10.1051/0004-6361/201833691
- Anderson, D. R., Brown, D. J. A., Collier Cameron, A. et al. 2014, *arXiv e-prints*, arXiv:1410.3449.
- Anderson, D. R., Collier Cameron, A., Hellier, C. et al. 2015, *A&A*, 575, A61. doi: 10.1051/0004-6361/201423591
- Bakos, G. Á. 2018, The HATNet and HATSouth Exoplanet Surveys. H. J. Deeg & J. A. Belmonte (Eds.), *Handbook of Exoplanets* p. 111. doi: 10.1007/978-3-319-55333-7_111
- Barge, P., Baglin, A., Auvergne, M., & CoRoT Team. 2008, CoRoT: pioneer space mission for exoplanet transit search. Y.-S. Sun, S. Ferraz-Mello, & J.-L. Zhou (Eds.), *Exoplanets: Detection, Formation and Dynamics* Vol. 249, p. 3-16. doi: 10.1017/S1743921308016293
- Barros, S. C. C., Brown, D. J. A., Hébrard, G. et al. 2016, *A&A*, 593, A113. doi: 10.1051/0004-6361/201526517
- Bodenheimer, P., Laughlin, G., & Lin, D. N. C. 2003, *ApJ*, 592(1), 555–563. Retrieved from <https://doi.org/10.1086/375565>
- Bodenheimer, P., Lin, D. N. C., & Mardling, R. A. 2001, *ApJ*, 548(1), 466-472. doi: 10.1086/318667
- Bohn, A. J., Southworth, J., Ginski, C., Kenworthy, M. A., Maxted, P. F. L., & Evans, D. F. 2020, *A&A*, 635, A73. doi: 10.1051/0004-6361/201937127
- Borucki, W. J., Koch, D., Basri, G. et al. 2010, *Science*, 327(5968), 977. doi: 10.1126/science.1185402
- Buchhave, L. A., Bakos, G. Á., Hartman, J. D. et al. 2010, *ApJ*, 720(2), 1118-1125. doi: 10.1088/0004-637X/720/2/1118
- Burrows, A. S. 2014, *Nature*, 513(7518), 345-352. doi: 10.1038/nature13782
- Ciardi, D. R., Beichman, C. A., Horch, E. P., & Howell, S. B. 2015, *ApJ*, 805(1), 16. doi: 10.1088/0004-637X/805/1/16
- Ciceri, S., Mancini, L., Southworth, J. et al. 2013, *A&A*, 557, A30. doi: 10.1051/0004-6361/201321669
- Claret, A. 2017, *A&A*, 600, A30. doi: 10.1051/0004-6361/201629705
- Eastman, J., Siverd, R., & Gaudi, B. S. 2010, *PASP*, 122(894), 935. doi: 10.1086/655938
- Ehrenreich, D., Lovis, C., Allart, R. et al. 2020, *Nature*, 580(7805), 597-601. doi: 10.1038/s41586-020-2107-1
- Espinoza, N., Brahm, R., Henning, T. et al. 2020, *MNRAS*, 491(2), 2982-2999. doi: 10.1093/mnras/stz3150
- Evans, D. F., Southworth, J., & Smalley, B. 2016, *ApJ*, 833(2), L19. doi: 10.3847/2041-8213/833/2/L19
- Foreman-Mackey, D., Hogg, D. W., Lang, D., & Goodman, J. 2013, *PASP*, 125(925), 306. doi: 10.1086/670067
- Fortney, J. J., Marley, M. S., & Barnes, J. W. 2007, *ApJ*, 659(2), 1661-1672. doi: 10.1086/512120
- Gajdoš, P., Vaňko, M., Jakubík, M. et al. 2019, *MNRAS*, 485(3), 3580-3587. doi: 10.1093/mnras/stz676
- Gardner, J. P., Mather, J. C., Clampin, M. et al. 2006, *Space Sci. Rev.*, 123(4), 485-606. doi: 10.1007/s11214-006-8315-7
- Guerrero, N. M., Seager, S., Huang, C. X. et al. 2021, *ApJS*, 254(2), 39. doi: 10.3847/1538-4365/abefe1
- Guillot, T., & Showman, A. P. 2002, *A&A*, 385, 156-165. doi: 10.1051/0004-6361:20011624
- Hay, K. L., Collier-Cameron, A., Doyle, A. P. et al. 2016, *MNRAS*, 463(3), 3276-3289. doi: 10.1093/mnras/stw2090
- Hellier, C., Anderson, D. R., Bouchy, F. et al. 2019, *MNRAS*, 482(1), 1379-1391. doi: 10.1093/mnras/sty2741
- Hellier, C., Anderson, D. R., Collier Cameron, A. et al. 2017, *MNRAS*, 465(3), 3693-3707. doi: 10.1093/mnras/stw3005
- Howarth, I. D. 2011, *MNRAS*, 418(2), 1165-1175. doi: 10.1111/j.1365-2966.2011.19568.x
- Howell, S. B., Sobock, C., Haas, M. et al. 2014, *PASP*, 126(938), 398. doi: 10.1086/676406
- Jenkins, J. M., Twicken, J. D., McCauliff, S. et al. 2016, The TESS science processing operations center. G. Chiozzi & J. C. Guzman (Eds.), *Software and Cyberinfrastructure for Astronomy IV* Vol. 9913, pp. 1232 – 1251. SPIE. Retrieved from <https://doi.org/10.1117/12.2233418>
- Kreidberg, L. 2015, *PASP*, 127(957), 1161. doi: 10.1086/683602
- Lam, K. W. F., Faedi, F., Brown, D. J. A. et al. 2017, *A&A*, 599, A3. doi: 10.1051/0004-6361/201629403
- Laughlin, G., Crismani, M., & Adams, F. C. 2011, *ApJ*, 729(1), L7. doi: 10.1088/2041-8205/729/1/L7
- Leconte, J., Chabrier, G., Baraffe, I., & Levrard, B. 2010, *A&A*, 516, A64. doi: 10.1051/0004-6361/201014337
- Lightkurve Collaboration, Cardoso, J. V. d. M., Hedges, C. et al. 2018, Lightkurve: Kepler and TESS time series analysis in Python., *Astrophysics Source Code Library*.
- Littlefield, C., Garnavich, P., Mukai, K. et al. 2019, *ApJ*, 881(2), 141. doi: 10.3847/1538-4357/ab2a17

- Mallonn, M., Bernt, I., Herrero, E. et al. 2016, *MNRAS*, 463(1), 604-614. doi: 10.1093/mnras/stw1999
- Mallonn, M., Nascimbeni, V., Weingrill, J. et al. 2015, *A&A*, 583, A138. doi: 10.1051/0004-6361/201425395
- Mallonn, M., Poppenhaeger, K., Granzer, T., Weber, M., & Strassmeier, K. G. 2021, *arXiv e-prints*, arXiv:2110.14344.
- Miller, N., & Fortney, J. J. 2011, *ApJ*, 736(2), L29. doi: 10.1088/2041-8205/736/2/L29
- Morris, B. M., Agol, E., Hebb, L., & Hawley, S. L. 2018, *AJ*, 156(3), 91. doi: 10.3847/1538-3881/aad3b7
- Oshagh, M., Santos, N. C., Boisse, I., Boué, G., Montalto, M., Dumusque, X., & Haghighipour, N. 2013, *A&A*, 556, A19. doi: 10.1051/0004-6361/201321309
- Parviainen, H., Palle, E., Zapatero-Osorio, M. R. et al. 2021, *A&A*, 645, A16. doi: 10.1051/0004-6361/202038934
- Poppenhaeger, K., & Wolk, S. J. 2014, *A&A*, 565, L1. doi: 10.1051/0004-6361/201423454
- Rauer, H., Catala, C., Aerts, C. et al. 2014, *Experimental Astronomy*, 38(1-2), 249-330. doi: 10.1007/s10686-014-9383-4
- Ricker, G. R., Winn, J. N., Vanderspek, R. et al. 2015, *Journal of Astronomical Telescopes, Instruments, and Systems*, 1, 014003. doi: 10.1117/1.JATIS.1.1.014003
- Ridden-Harper, A., Turner, J. D., & Jayawardhana, R. 2020, *AJ*, 160(6), 249. doi: 10.3847/1538-3881/abba1e
- Schwarz, G. 1978, *The Annals of Statistics*, 6(2), 461-464. Retrieved from <http://www.jstor.org/stable/2958889>
- Seager, S. 2011, Exoplanet atmospheres: A theoretical outlook. A. Sozzetti, M. G. Lattanzi, & A. P. Boss (Eds.), *The Astrophysics of Planetary Systems: Formation, Structure, and Dynamical Evolution* Vol. 276, p. 198-207. doi: 10.1017/S1743921311020187
- Seager, S., & Mallén-Ornelas, G. 2003, On the Unique Solution of Planet and Star Parameters from an Extrasolar Planet Transit Light Curve. D. Deming & S. Seager (Eds.), *Scientific Frontiers in Research on Extrasolar Planets* Vol. 294, p. 419-422.
- Shporer, A., Wong, I., Huang, C. X. et al. 2019, *AJ*, 157(5), 178. doi: 10.3847/1538-3881/ab0f96
- Sing, D. K., Fortney, J. J., Nikolov, N. et al. 2016, *Nature*, 529, 59-62. doi: 10.1038/nature16068
- Southworth, J., Bohn, A. J., Kenworthy, M. A., Ginski, C., & Mancini, L. 2020, *A&A*, 635, A74. doi: 10.1051/0004-6361/201937334
- Southworth, J., Mancini, L., Novati, S. C. et al. 2010, *MNRAS*, 408, 1680-1688. doi: 10.1111/j.1365-2966.2010.17238.x
- Southworth, J., Wheatley, P. J., & Sams, G. 2007, *MNRAS*, 379, L11-L15. doi: 10.1111/j.1745-3933.2007.00324.x
- Strassmeier, K. G., Granzer, T., Weber, M. et al. 2004, *Astronomische Nachrichten*, 325, 527-532. doi: 10.1002/asna.200410273
- Strassmeier, K. G., Granzer, T., Weber, M. et al. 2010, *Advances in Astronomy*, 2010, 970306. doi: 10.1155/2010/970306
- Street, R. A., Pollaco, D. L., Fitzsimmons, A. et al. 2003, Super-WASP: Wide Angle Search for Planets. D. Deming & S. Seager (Eds.), *Scientific Frontiers in Research on Extrasolar Planets* Vol. 294, p. 405-408.
- Tenenbaum, P., & Jenkins, J. 2018, TESS Science Data Products Description Document, EXP-TESS-ARC-ICD-0014 Rev D., <https://archive.stsci.edu/missions/tess/doc/EXP-TESS-ARC-ICD-TM-0014.pdf>.
- Thompson, S. E., Fraquelli, D., Van Cleve, J. E., & Caldwell, D. A. 2016, Kepler Archive Manual., Kepler Science Document KDMC-10008-006.
- Turner, J. D., Ridden-Harper, A., & Jayawardhana, R. 2021, *AJ*, 161(2), 72. doi: 10.3847/1538-3881/abd178
- Turner, O. D., Anderson, D. R., Barkaoui, K. et al. 2019, *MNRAS*, 485(4), 5790-5799. doi: 10.1093/mnras/stz742
- Turner, O. D., Anderson, D. R., Collier Cameron, A. et al. 2016, *PASP*, 128(964), 064401. doi: 10.1088/1538-3873/128/964/064401
- von Essen, C., Mallonn, M., Hermansen, S., Nixon, M. C., Madhusudhan, N., Kjeldsen, H., & Tautvaišienė, G. 2020, *arXiv e-prints*, arXiv:2003.06424.
- West, R. G., Hellier, C., Almenara, J. M. et al. 2016, *A&A*, 585, A126. doi: 10.1051/0004-6361/201527276
- Winn, J. N., Johnson, J. A., Howard, A. W. et al. 2010, *ApJ*, 718(1), 575-582. doi: 10.1088/0004-637X/718/1/575
- Wong, I., Kitzmann, D., Shporer, A. et al. 2021, *AJ*, 162(4), 127. doi: 10.3847/1538-3881/ac0c7d
- Yip, K. H., Changeat, Q., Edwards, B. et al. 2021, *AJ*, 161(1), 4. doi: 10.3847/1538-3881/abc179

How cite this article: X. Alexoudi (2021), On the parameter refinement of inflated exoplanets with large radius uncertainty based on TESS observations, *ASNA*, .

APPENDIX A: BEST FIT TRANSIT MODELS AND CORNER PLOTS FOR ALL THE FIT PARAMETERS.

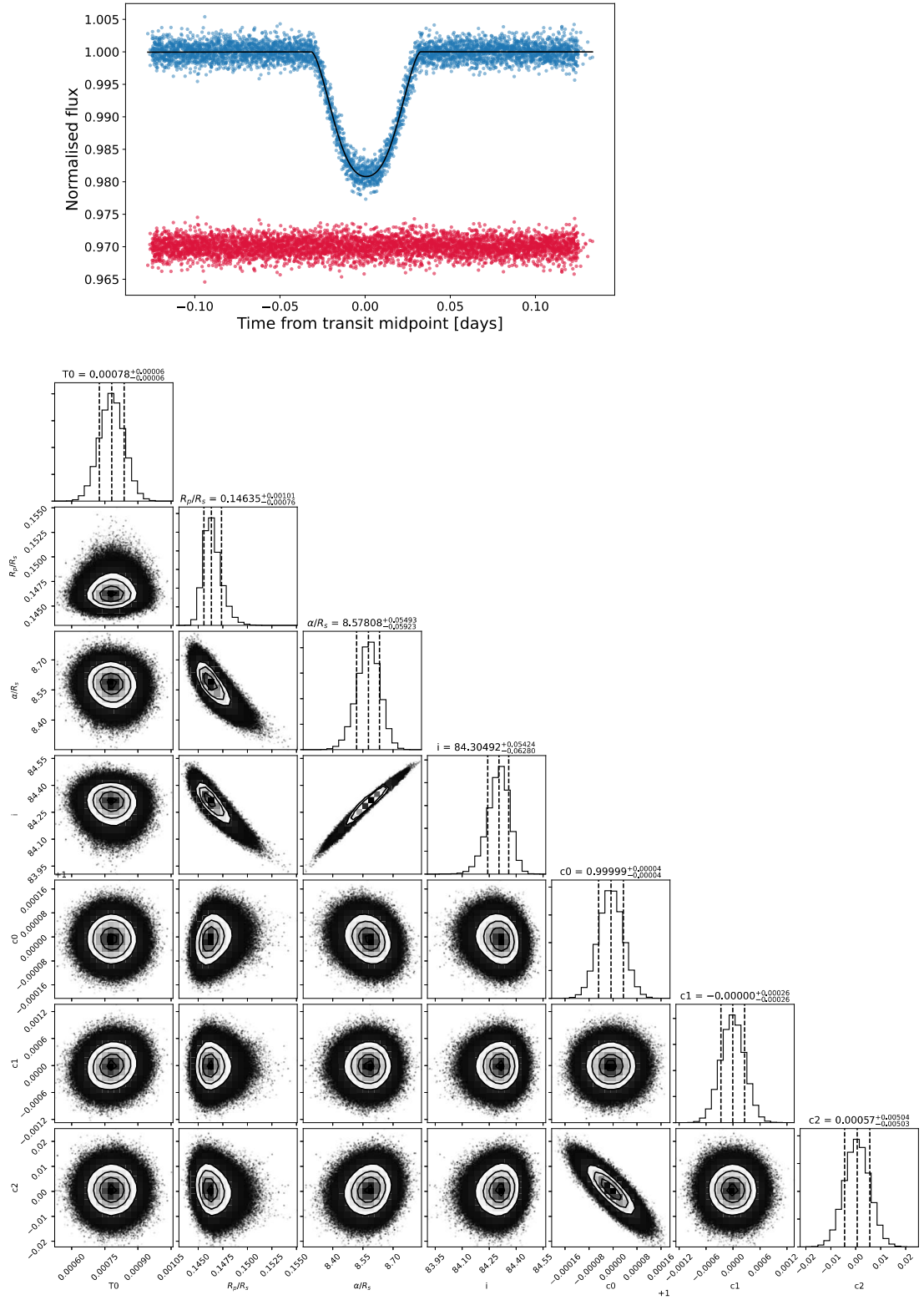


FIGURE A1 In the upper panel, we show the folded TESS light curves of WASP-140 b (blue dots) along with the best fit transit model (black solid line). The residuals are presented with red dots and an offset for clarity. In the lower panel, we show the corner plot of the best fit parameters. It is the 2D projection of the sample plotted in a way to show covariance between the parameters.

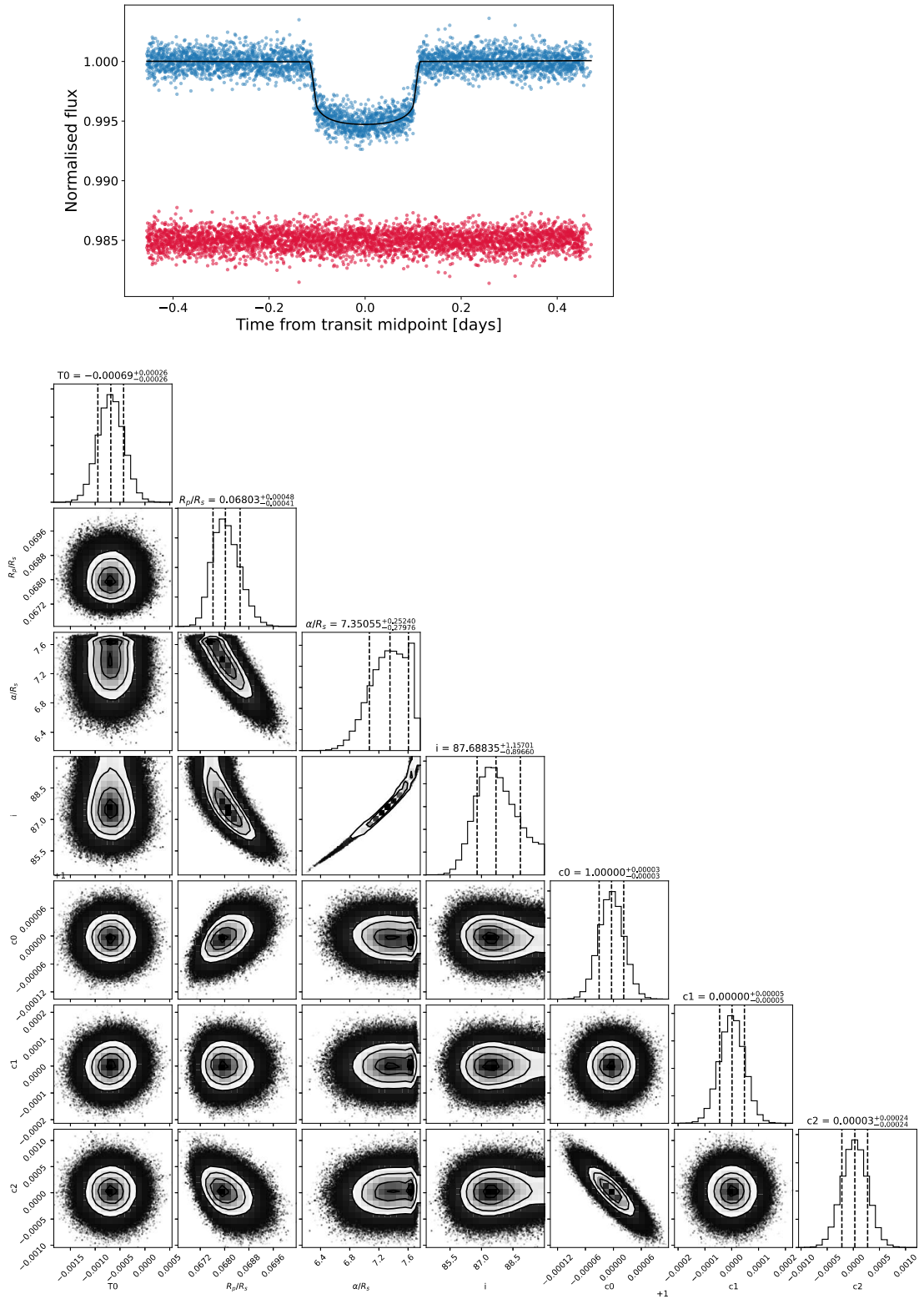


FIGURE A2 The same as Fig. A1 , but for the exoplanet WASP-136 b.

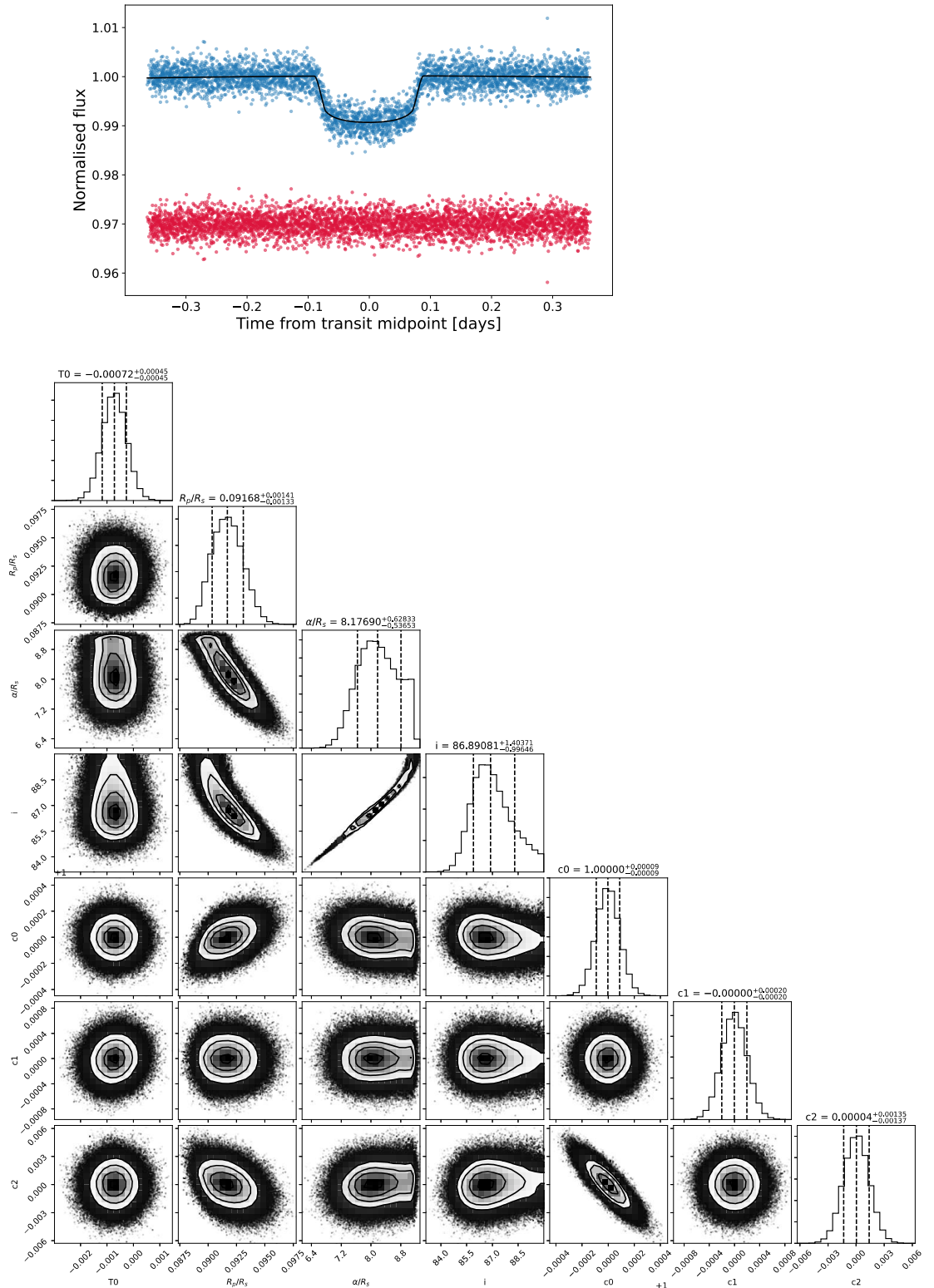


FIGURE A3 The same as Fig. A1 , but for the exoplanet WASP-113 b.

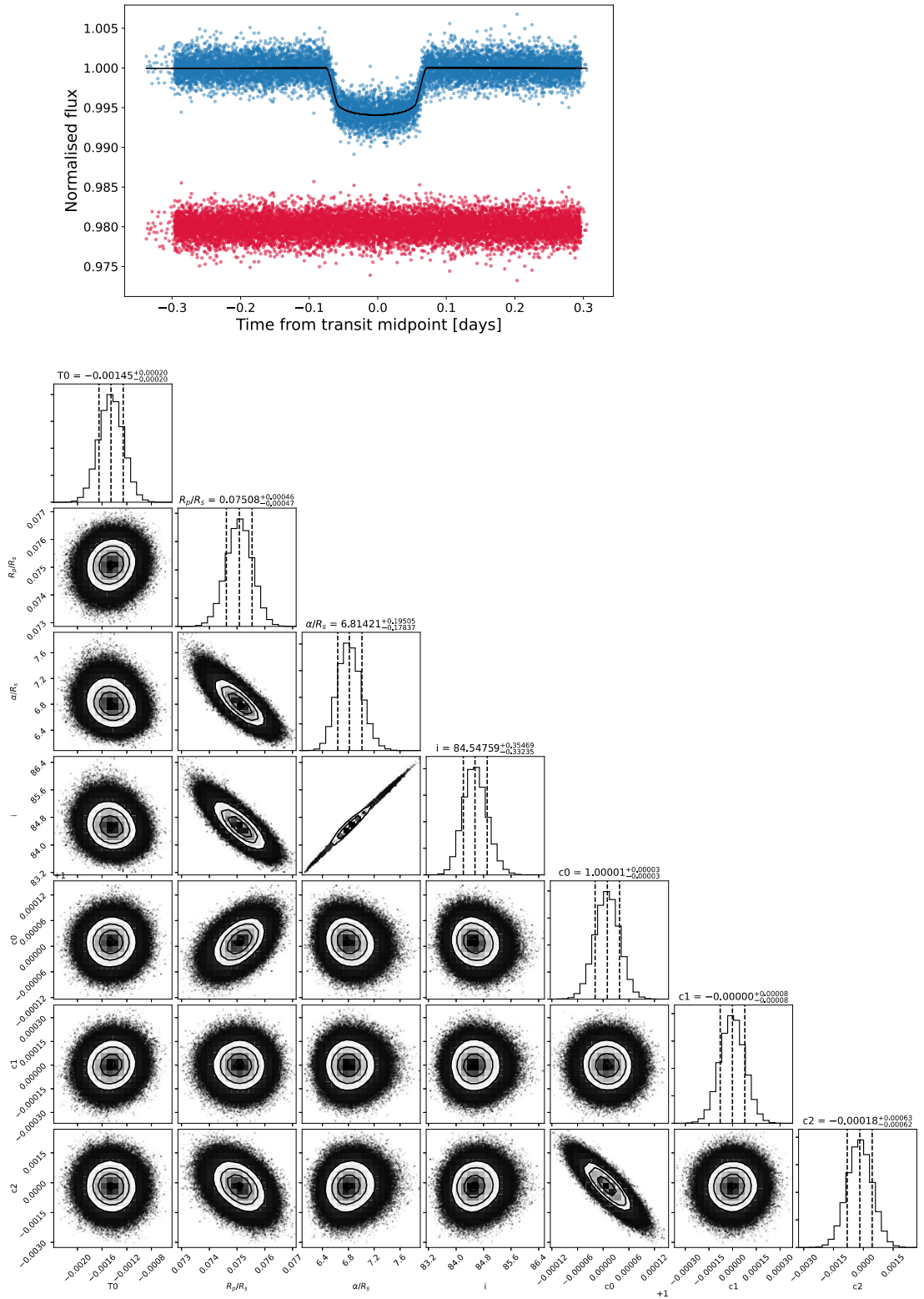


FIGURE A4 The same as Fig. A1 , but for the exoplanet WASP-120 b.

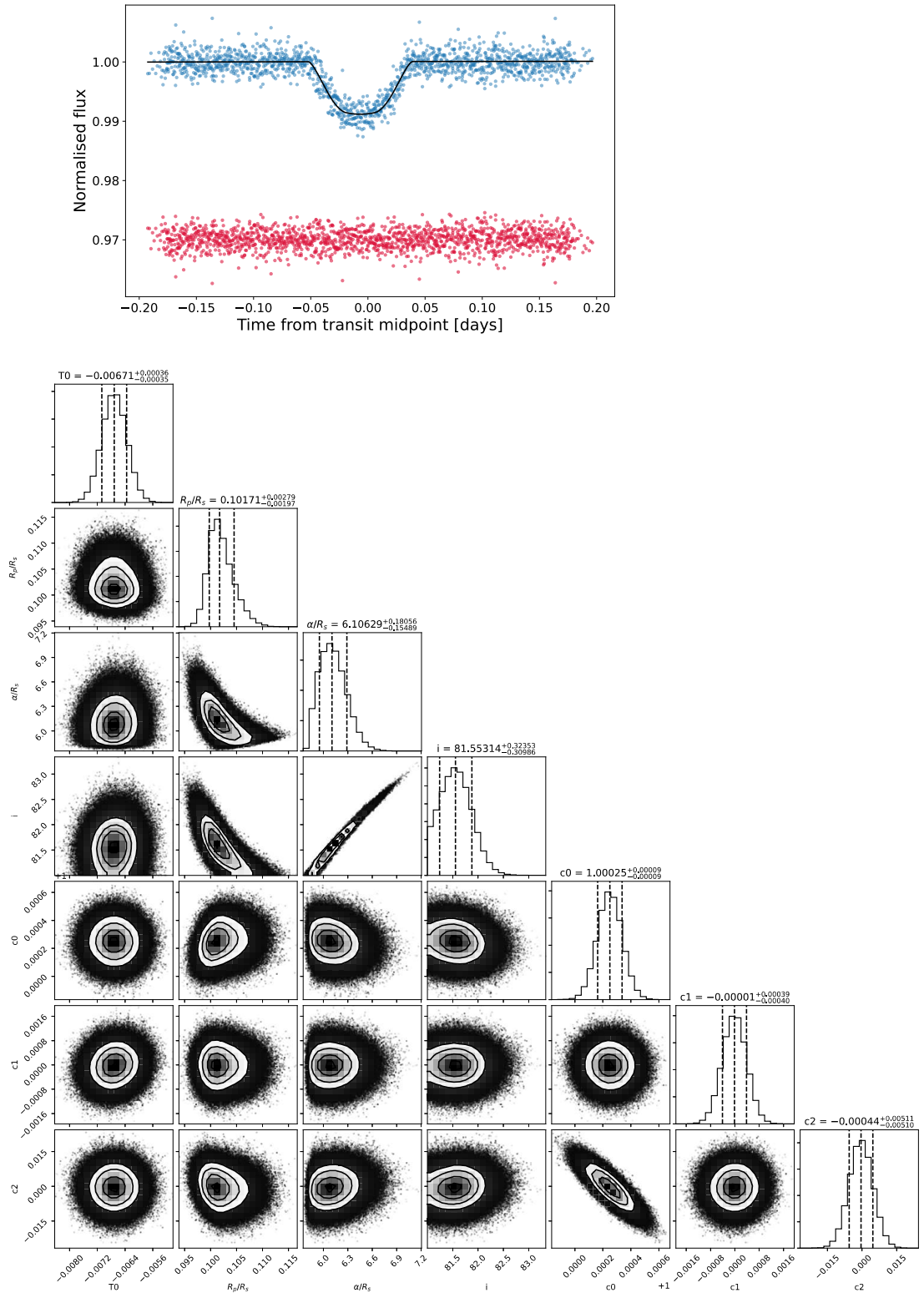


FIGURE A5 The same as Fig. A1, but for the exoplanet WASP-93 b.

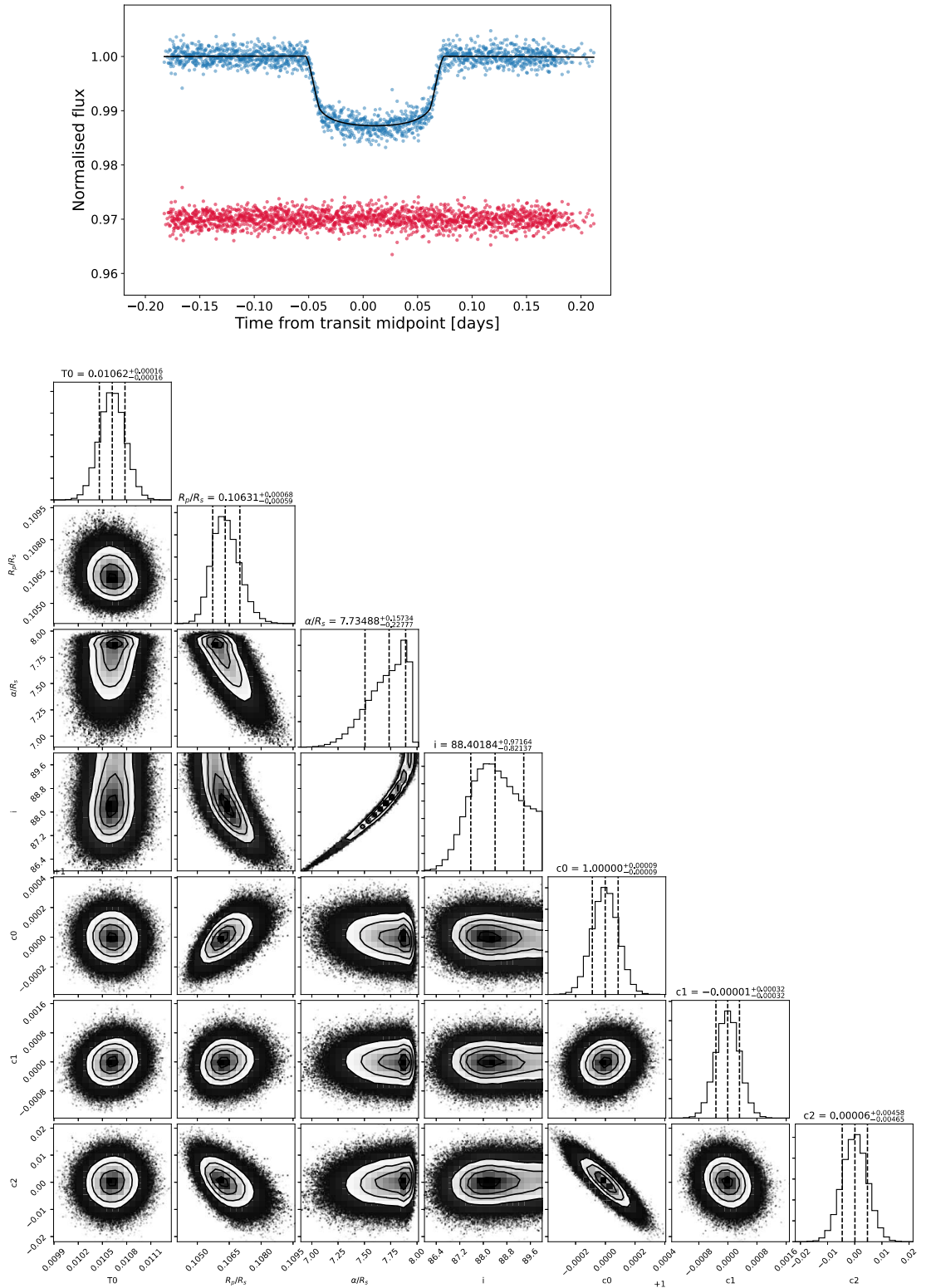


FIGURE A6 The same as Fig. A1, but for the exoplanet HAT-P-16 b.

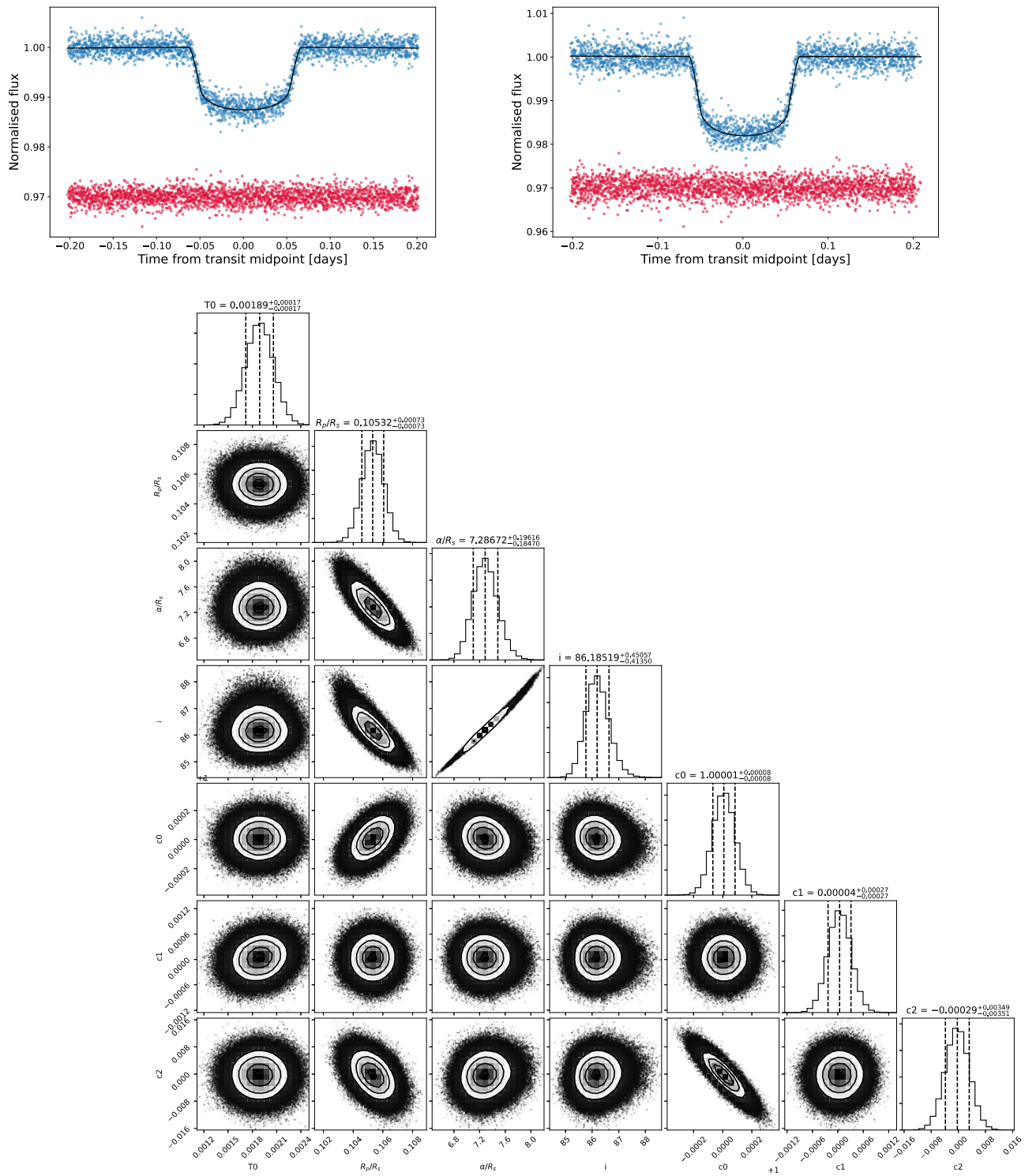


FIGURE A7 Best fit transit model for the TESS light curves of WASP-123 b. On the upper left panel there are observations from sector 27 and on the upper right panel from sector 13. On the lower panel, the corner plot of the best fit parameters for WASP-123 b.

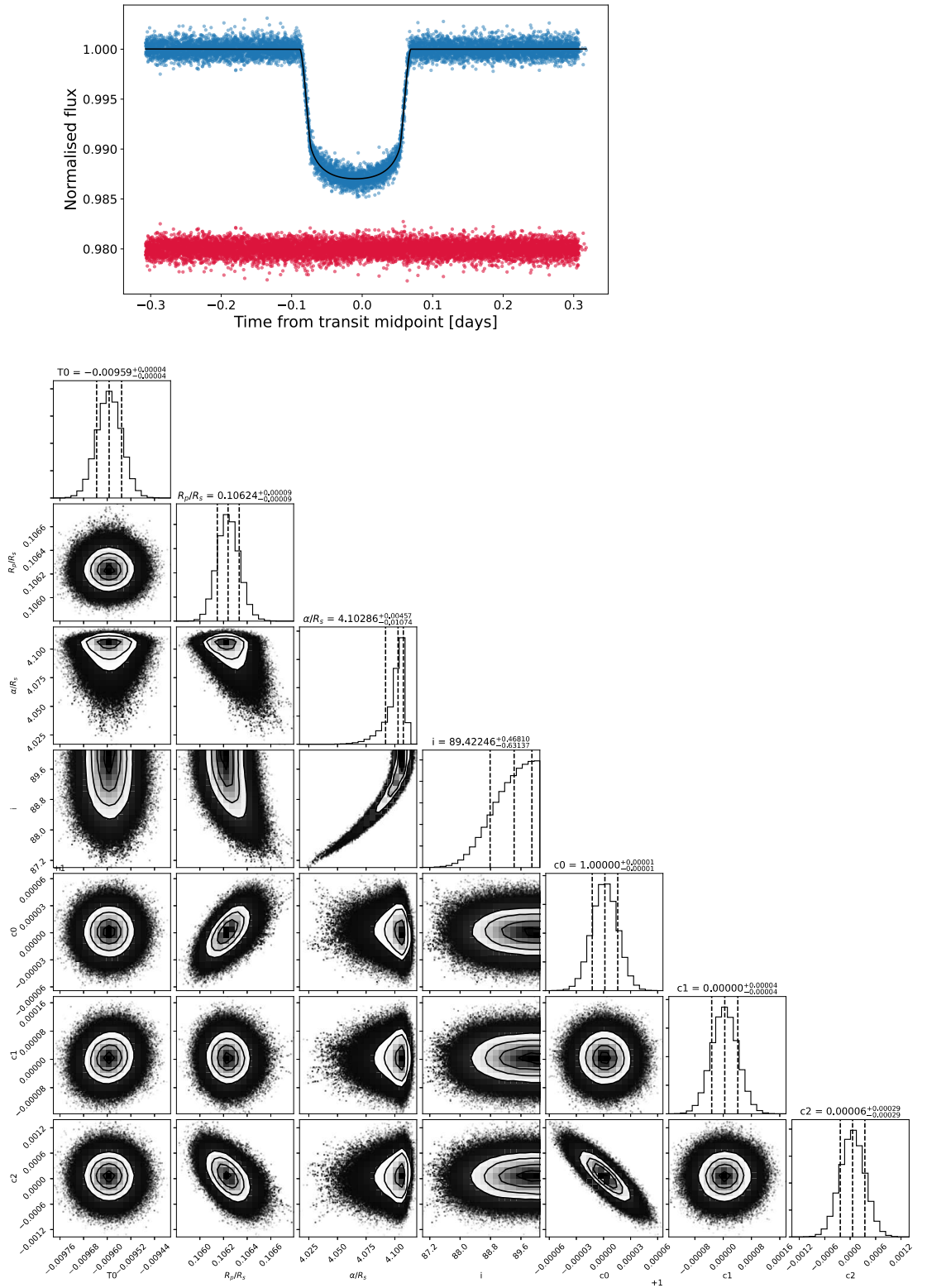


FIGURE A8 The same as Fig. A1, but for the exoplanet WASP-76 b.

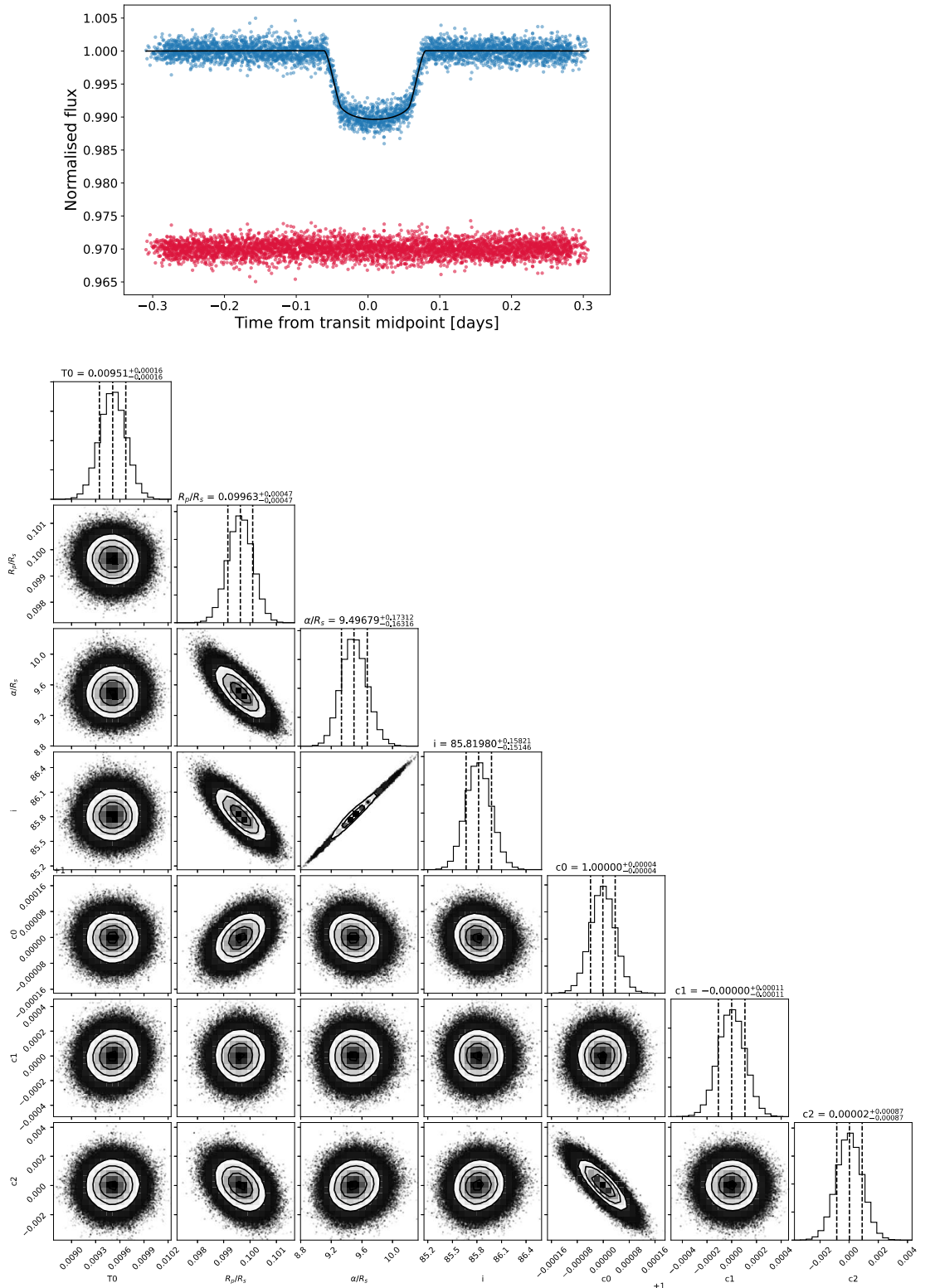


FIGURE A9 The same as Fig. A1, but for the exoplanet WASP-20 b.

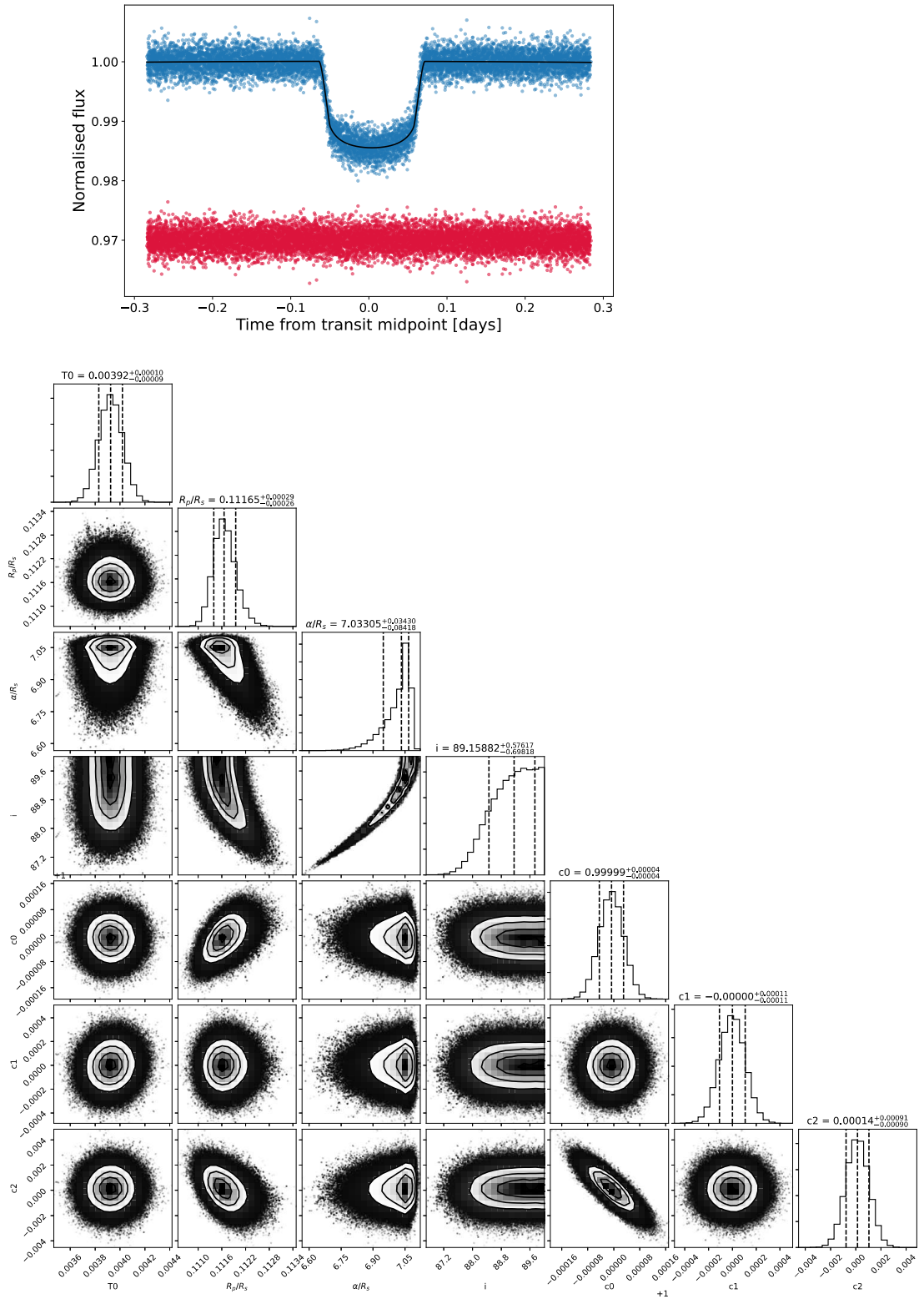


FIGURE A10 The same as Fig. A1, but for the exoplanet WASP-108 b.